

DISEASES AND DISORDERS

Proline metabolic reprogramming modulates cardiac remodeling induced by pressure overload in the heart

Qingbo Lv^{1†}, Duanbin Li^{1†}, Liding Zhao², Pengcheng Yu¹, Yecheng Tao¹, Qiongjun Zhu¹, Yao Wang¹, Meihui Wang¹, Guosheng Fu^{1*}, Min Shang^{1*}, Wenbin Zhang^{1*}

Metabolic reprogramming is critical in the onset of pressure overload–induced cardiac remodeling. Our study reveals that proline dehydrogenase (PRODH), the key enzyme in proline metabolism, reprograms cardiomyocyte metabolism to protect against cardiac remodeling. We induced cardiac remodeling using transverse aortic constriction (TAC) in both cardiac-specific PRODH knockout and overexpression mice. Our results indicate that PRODH expression is suppressed after TAC. Cardiac-specific PRODH knockout mice exhibited worsened cardiac dysfunction, while mice with PRODH overexpression demonstrated a protective effect. In addition, we simulated cardiomyocyte hypertrophy in vitro using neonatal rat ventricular myocytes treated with phenylephrine. Through RNA sequencing, metabolomics, and metabolic flux analysis, we elucidated that PRODH overexpression in cardiomyocytes redirects proline catabolism to replenish tricarboxylic acid cycle intermediates, enhance energy production, and restore glutathione redox balance. Our findings suggest PRODH as a modulator of cardiac bioenergetics and redox homeostasis during cardiac remodeling induced by pressure overload. This highlights the potential of PRODH as a therapeutic target for cardiac remodeling.

INTRODUCTION

Hypertension, the most prevalent cardiovascular disorder worldwide, profoundly threatens cardiac health without proper management (1). In the early stages of elevated cardiac afterload caused by sustained hypertension, the heart undergoes myocardial hypertrophy, a pathological condition characterized by abnormal enlargement of cardiomyocytes. As the disease advances, compensatory cardiac hypertrophy is followed by disrupted myocardial structure, impeded blood supply, and compromised cardiac function, ultimately culminating in heart failure (HF) or cardiac death (2–4). Presently, therapeutic options for addressing maladaptive cardiac remodeling remain restricted, with a conspicuous absence of modalities capable of either delaying or reversing such pathological processes (5). Therefore, comprehensive studies to uncover the pathological mechanism of cardiac hypertrophy and identify appropriate targets to delay or reverse cardiac hypertrophy might pave the way to prevent HF.

The heart is one of the most metabolically active organs in the body. Before the onset of structural cardiac remodeling, the heart undergoes metabolic adaptation to meet heightened energy requisites during the cardiac hypertrophy. The metabolic remodeling of the heart can assist cardiomyocytes in coping with relative energy insufficiency and imbalanced redox homeostasis (6–8). Metabolic remodeling precedes cardiac dysfunction. Regulating the metabolic remodeling of cardiomyocytes can effectively prevent pathological progression in the early stages of remodeling (9). Previous studies have demonstrated that reprogramming cardiomyocyte metabolism can preserve cardiac function during pressure overload–induced cardiac remodeling and prevent HF (10–12). These investigations primarily focused on regulating glycolysis and fatty acid oxidation

of cardiomyocytes to achieve the alleviation of cardiac remodeling. In sharp contrast, there is relatively limited research on elucidating the role of amino acid metabolism in cardiac remodeling. Nevertheless, the precise metabolic alterations and underlying mechanisms of amino acid metabolism during cardiac remodeling remain largely elusive.

Proline, a non-essential amino acid, not only serves as a fundamental element for protein synthesis but also participates in diverse cellular processes critical for cell survival and adaptation (13). Emerging studies have elucidated its multifaceted functions, including its involvement in redox balance regulation and energy metabolism modulation (14–16). Hence, alterations in proline metabolism might have been implicated in the pathogenesis of various diseases. Unraveling its intricate network of interactions within cellular metabolism holds promise for therapeutic interventions targeting a wide array of pathological conditions. Proline dehydrogenase (PRODH), the first enzyme in proline catabolism, has been reported to be the most crucial enzyme in regulating proline metabolism (17). PRODH catalyzes the conversion of proline to pyrroline-5-carboxylate, further converting to glutamate or ornithine (18). Previous studies have noticed the changes of proline metabolism during myocardial remodeling (9, 19). However, detailed studies are needed to investigate how the alternation of proline metabolism links to cardiac performance.

In the present study, we primarily investigated the role of PRODH in pressure overload–induced cardiac remodeling. We aimed to elucidate the crucial role of PRODH in maintaining cardiac function in transverse aortic constriction (TAC)–induced pathological cardiac remodeling using a genetic approach. Furthermore, we confirmed that cardiac specific overexpression of PRODH exerted a protective effect on cardiac function and inhibited adverse myocardial remodeling. Mechanistically, we demonstrated that promoting proline catabolism can restore energy and redox balance in cardiomyocytes. These findings collectively demonstrate the critical regulatory role of PRODH in cardiac remodeling. Our results provide insights into the metabolic mechanisms of HF and propose a potential target for future therapeutic interventions.

¹Key Laboratory of Cardiovascular Intervention and Regenerative Medicine of Zhejiang Province, Department of Cardiology, Sir Run Run Shaw Hospital, School of Medicine, Zhejiang University, Hangzhou, China. ²Department of Cardiology, The First Affiliated Hospital, School of Medicine, Zhejiang University, Hangzhou, China.

*Corresponding author. Email: fugs@zju.edu.cn (G.F.); minshang@zju.edu.cn (M.S.); 3313011@zju.edu.cn (W.Z.)

†These authors contributed equally to this work.

RESULTS

The expression of PRODH was decreased in the hypertrophic hearts

We started by assessing the relevance of PRODH in pathological cardiac remodeling. To achieve this, we first examined the expression levels of PRODH in HF and hypertrophic cardiomyopathy (HCM) by using two public RNA sequencing (RNA-seq) datasets: GSE141910 and GSE133054. We found that the expression of PRODH was markedly down-regulated in hearts of both HF and HCM (Fig. 1, A and B). Following this, we sought to explore the changes in PRODH expression during TAC-induced cardiac remodeling in mice. We conducted a time course single-cell RNA-seq analysis on mouse hearts (0, 3 days, 1 week, and 4 weeks) following TAC-induced pressure overload using the public dataset GSE95143 (Fig. 1C). Consistent with our previous findings, PRODH expression was markedly reduced on 3 days, 1 week, and 4 weeks after TAC (Fig. 1D). Furthermore, we established a murine

model of cardiac hypertrophy by performing TAC surgery. After 4 weeks, we harvested the heart tissue and found that the expression levels of PRODH were substantially down-regulated at both mRNA and protein levels in the hearts of TAC mice compared to sham (Fig. 1, E to G). In line with this, PRODH activity was reduced in the hearts upon TAC (Fig. 1H). Previous studies has indicated that TAC surgery activates the mammalian target of rapamycin (mTOR) pathway (20, 21), which is known to negatively regulate PRODH expression (15, 17). To elucidate the mechanisms underlying the decreased expression of PRODH following TAC surgery, we collected cardiac tissue samples from mice treated with 4 weeks of rapamycin or saline after TAC surgery. We observed a notable increase in PRODH expression in the group treated with rapamycin, suggesting a link between mTOR activation and PRODH expression following TAC surgery (fig. S1, A to D). Next, to mimic in vitro cardiomyocyte remodeling, we treated neonatal rat ventricular myocytes (NRVMs)

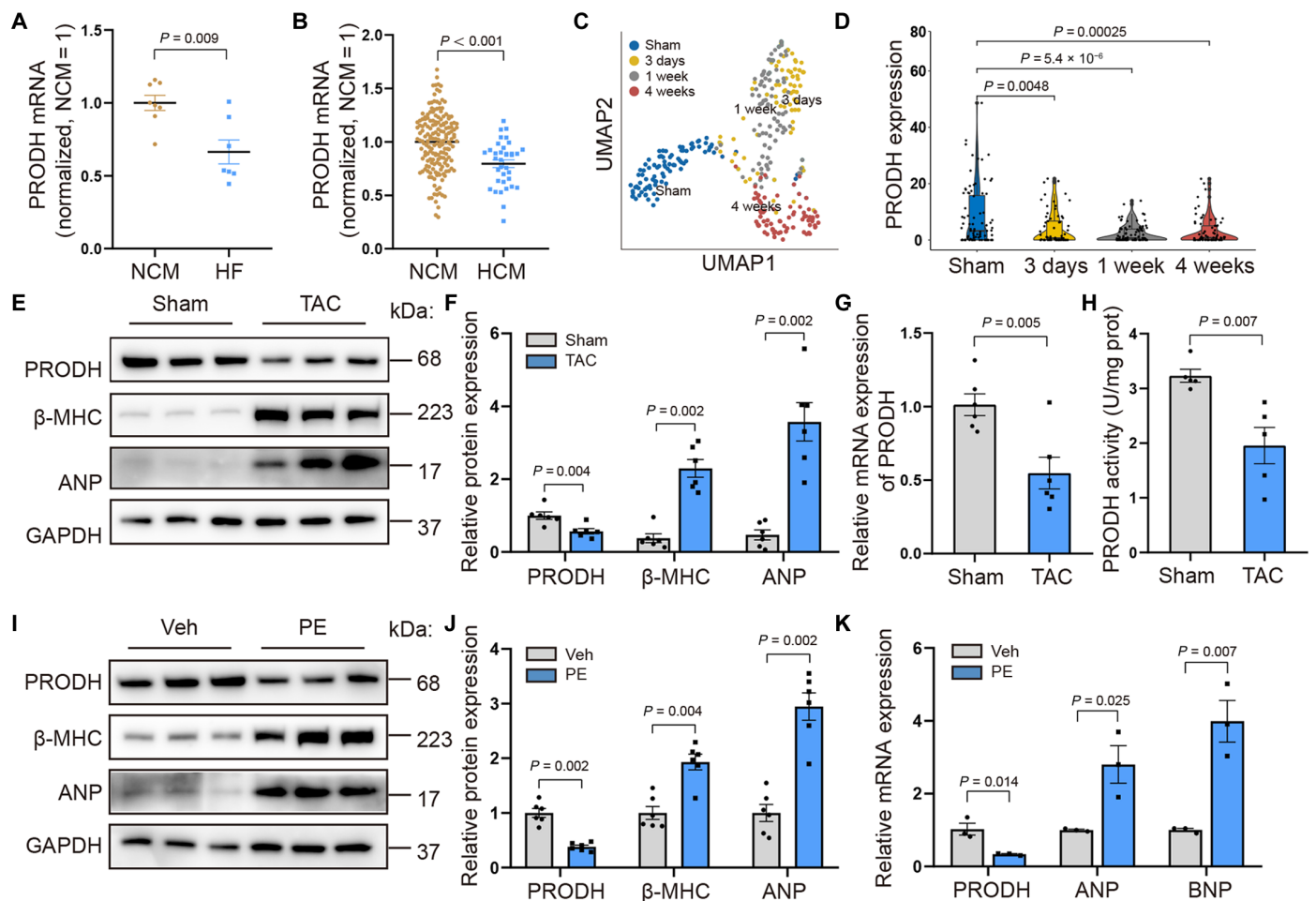


Fig. 1. PRODH expression was decreased in hypertrophic hearts. (A) The mRNA expression of PRODH in heart tissues from patients with HF and normal cardiac myocytes (NCM) in the RNA-seq database GSE133054 ($n = 7$ for HF; $n = 8$ for NCM). (B) The mRNA expression of PRODH in heart tissues from patients with HCM and NCM by combining the RNA-seq database GSE141910 and GSE133054 ($n = 174$ for HCM; $n = 36$ for NCM). (C and D) The clustering diagram and relative PRODH expression after TAC acquired by single-cardiomyocyte RNA-seq of dataset GSE95143. (E and F) Representative images and quantification of PRODH, β -MHC, and ANP protein levels measured by Western blotting in heart tissues from sham and TAC-operated mice ($n = 6$). GAPDH, glyceraldehyde-3-phosphate dehydrogenase. (G and H) Relative mRNA and enzyme activity of PRODH in heart tissues from sham and TAC-operated mice ($n = 6$). (I and J) Representative images and quantification of PRODH, β -MHC, and ANP protein levels measured by Western blotting in isolated NRVMs stimulated with PE (100 μ M) or vehicle (Veh) for 48 hours ($n = 6$). (K) Quantification of mRNA expression of PRODH, ANP, and BNP by reverse transcription-quantitative polymerase chain reaction (RT-qPCR) in isolated NRVMs stimulated with PE (100 μ M) or vehicle for 48 hours ($n = 3$). (Data are shown as means \pm SEM. Unpaired two-tailed Student's *t* test was conducted for the comparison.)

with pro-hypertrophic stimuli, phenylephrine (PE). Consistent with our *in vivo* results, both mRNA and protein expression were notably decreased in PE-induced hypertrophic cardiomyocytes (Fig. 1, I to K). Overall, these data demonstrated that both the expression level and the activity of PRODH were reduced in hypertrophic cardiomyocytes.

PRODH deficiency aggravated the adverse cardiac remodeling induced by TAC in mice

To investigate the role of PRODH in pressure overload-induced cardiac remodeling, cardiac-specific PRODH conditional knockout (cKO) mice were generated by intercrossing *Prodh* floxed mice with the α -myosin heavy chain promoter-driven Cre transgenic line. Subsequently, we performed TAC surgery on cKO mice and conducted echocardiographic analysis 4 weeks after surgery, and their littermates were used as controls (*f/f*). Cardiac-specific PRODH knockout mice markedly exacerbated TAC-induced cardiac dysfunction and show reduced ejection fraction (EF) and fractional shortening (FS) compared to *f/f* mice (Fig. 2, A to C), while no differences were observed in the survival rates between two strains (fig. S2A). In addition, cKO mice remarkably increased the left ventricular internal diameter at end-diastole (LVIDd) and left ventricular internal diameter at end-systole (LVIDs), suggesting left ventricular chamber dilation in cKO mice upon TAC (Fig. 2, D and E). Notably, the heart function and left ventricular diameters were comparable between *f/f* and cKO mice subjected to sham operations, indicating that cardiac-specific knocking out PRODH did not show any structural or function deficiencies at baseline. As anticipated, cKO mice showed higher heart weight/body weight (HW/BW) and heart weight/tibia length (HW/TL) ratios than *f/f* mice (Fig. 2, F and G), indicating aggravated cardiac remodeling. Next, we performed histology analysis on the mice's hearts upon TAC or sham. Hematoxylin and eosin (H&E) staining showed that cKO mouse hearts were larger and had a greater surface area (Fig. 2H). Masson's staining showed that cKO mice had considerably higher levels of cardiac fibrosis than *f/f* mice after TAC (Fig. 2I). Wheat germ agglutinin (WGA) staining revealed that the cross-sectional area of cKO mouse hearts was larger than that of *f/f* mice (Fig. 2J). Dihydroethidium (DHE) staining indicated that PRODH deficiency exacerbated oxidative damage in cardiomyocytes (Fig. 2K). Moreover, we isolated the adult mouse cardiac myocytes (AMCMs) and measured the reduced/oxidized glutathione (GSH/GSSG) ratio. Of note, cKO mice exhibited a more pronounced decrease in GSH/GSSG after TAC surgery compared to *f/f* mice (Fig. 2L), indicating a more severe impairment of antioxidant capacity in cKO mice upon TAC. Besides, the mRNA expression levels of the hypertrophic markers atrial natriuretic peptide (ANP), B-type natriuretic peptide (BNP), and β -myosin heavy chain (β -MHC), as well as the fibrotic markers collagen type 1a (Col1a), collagen type 3a (Col3a), and transforming growth factor- β (TGF β), were all increased in the hearts of cKO mice when compared with those in the *f/f* mice after TAC (Fig. 2, M and N). Consistently, the protein levels of β -MHC and ANP were also up-regulated in the cKO hearts (Fig. 2, O to R).

Given the elevated oxidative stress levels observed in cKO mice compared with *f/f* mice after TAC, we explored whether antioxidants could ameliorate cardiac functional deficits in cKO mice induced by TAC operation. Thus, we administered *N*-acetylcysteine (NAC) to cKO mice and assessed mouse cardiac function via echocardiography 4 weeks after surgery (fig. S3A). The results indicated that NAC treatment considerably enhanced cardiac function in cKO mice after

TAC, as evidenced by improved EF and FS (fig. S3, B and C). In addition, reduced LVIDd and LVIDs were observed in the cKO mice NAC-treated group, suggesting improved cardiac function (fig. S3, D and E). Consistently, cardiac hypertrophy indices, including HW/BW and HW/TL in cKO mice, were noticeably decreased following NAC administration (fig. S3, F and G). These results showed that antioxidant therapy with NAC partially reversed the impaired cardiac function in PRODH cKO mice. Collectively, cardiac PRODH deficiency accelerates adverse cardiac remodeling induced by pressure overload, with increased oxidative stress being a contributing factor.

Cardiac-specific overexpression of PRODH protected the heart from pressure overload-induced cardiac remodeling

To further explore the potential protective effects of cardiac-specific PRODH overexpression against TAC-induced cardiac remodeling, we used an adeno-associated virus 9 (AAV9) vector with a cardiac troponin T promoter to specifically overexpress PRODH in cardiomyocytes. In this mouse model featuring cardiac-specific PRODH overexpression (AAV9-PRODH), we performed TAC surgery and assessed cardiac function via echocardiography 4 weeks later. AAV9-PRODH mice showed preserved EF and FS upon TAC when compared to the AAV9-Vector injected mice as a control (Fig. 3, A to C). There were no substantive differences in the survival rates after TAC surgery between the AAV9-Vector mice and AAV9-PRODH mice (fig. S2B). In addition, while the control group exhibited increased LVIDd and LVIDs, indicative of ventricular dilation, these indicators were markedly reduced in the AAV9-PRODH mice (Fig. 3, D and E). Consistently, it was observed that the AAV9-PRODH mice exhibited decreased HW/BW and HW/TL ratios compared to the control group, indicating a reduction in cardiac hypertrophy (Fig. 3, F and G). Furthermore, Masson's staining showed that PRODH overexpression attenuated fibrosis induced by TAC operation, as demonstrated by Masson's staining (Fig. 3, H and I). In addition, WGA staining indicated a considerable reduction in the surface area of cardiomyocytes in TAC mice following PRODH overexpression (Fig. 3J), accompanied by a decrease in oxidative stress damage as evidenced by DHE staining (Fig. 3K). The GSH/GSSG ratio in isolated AMCMs from AAV9-PRODH mice was markedly enhanced compared to that of AAV9-Vector mice 4 weeks after TAC, indicating an improved antioxidant capacity of cardiomyocytes (Fig. 3L). To elucidate how PRODH overexpression affected the GSH/GSSG ratio, we examined the expression levels of enzymes involved in GSH metabolism within AMCMs. We observed a marked increase in glutathione reductase (GSR) expression after TAC, which was even more pronounced in AAV9-PRODH mice (fig. S4, A and B). Meanwhile, glutamate-cysteine ligase catalytic subunit (GCLC) expression remained unchanged in the TAC groups following PRODH overexpression (fig. S4C). These findings suggested that PRODH overexpression enhanced the GSH/GSSG ratio by modulating GSR activity, thereby promoting the reduction of GSSG to GSH in cardiomyocytes. Subsequently, we quantified mRNA levels of hypertrophic and fibrotic markers. The hypertrophic markers ANP, BNP, and β -MHC alongside fibrotic markers Col1a, Col3a, and TGF β were markedly elevated in the AAV9-Vector group after TAC but were notably suppressed in the AAV9-PRODH group (Fig. 3, M and N). Western blotting analysis further substantiated that PRODH overexpression in cardiomyocytes reduced the protein levels of hypertrophic markers following TAC (Fig. 3, O to R). Next, we assessed mitochondrial morphology within cardiac tissue sections. Mice subjected to sham surgery displayed

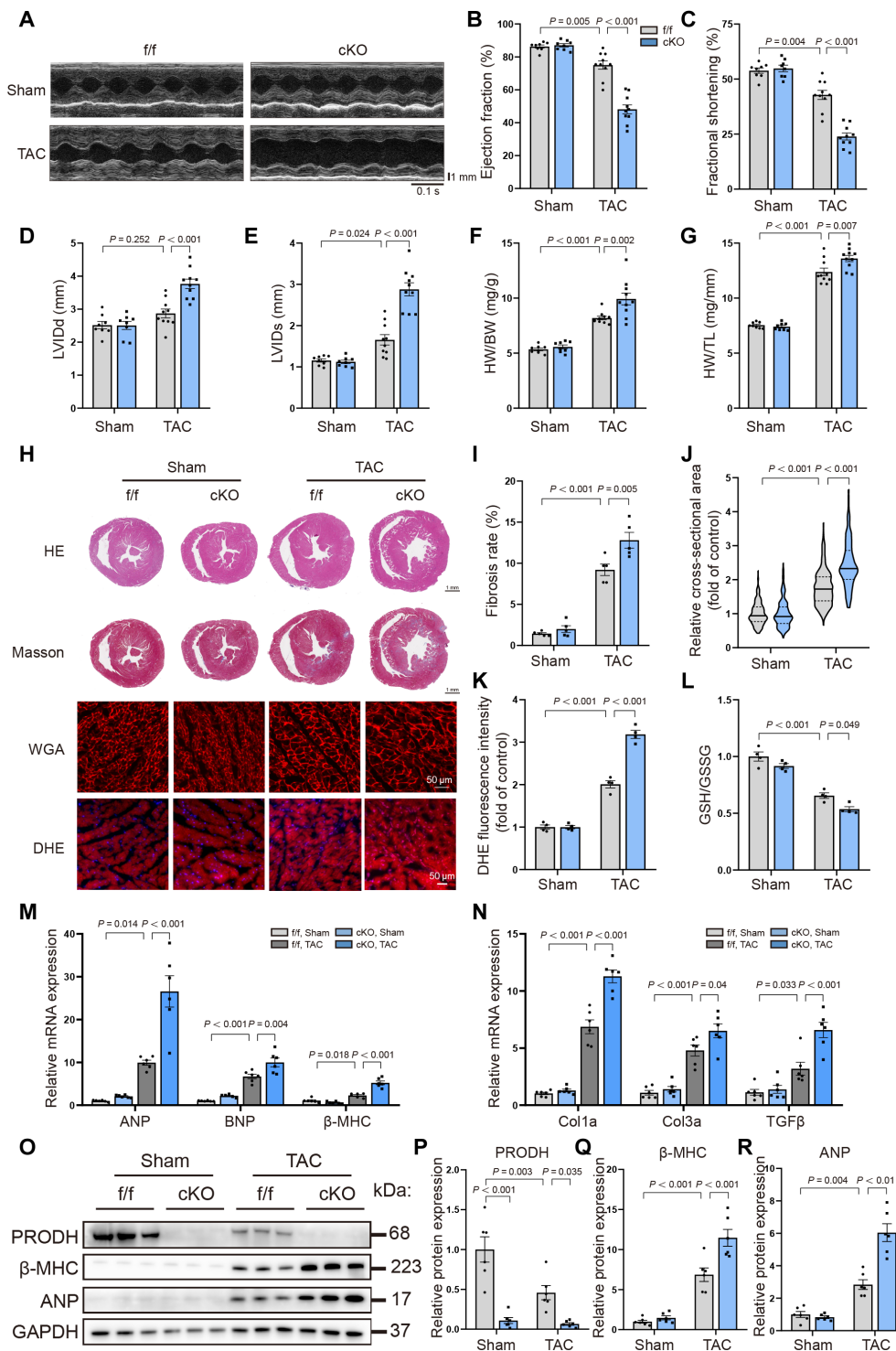


Fig. 2. Cardiac-specific deletion of PRODH aggravated adverse cardiac remodeling progression under pressure overload. (A to E) Representative M-mode echocardiography images and quantification of EF and FS, LVIDD, and LVIDs among the f/f and cKO mice after either sham or TAC ($n = 8$ for sham-operated mice; $n = 10$ for TAC-operated mice). (F and G) The ratios of HW/BW and HW/TL ($n = 8$ for sham-operated mice; $n = 10$ for TAC-operated mice). (H to K) Representative images of H&E staining, Masson's trichrome staining, WGA staining, and DHE and their quantitation results ($n = 5$ for each group of Masson's trichrome staining; $n = 256$ cells for each group of the WGA staining; $n = 4$ for DHE staining). (L) Relative GSH/GSSG ratio of AMCMs isolated from the in vivo experiment ($n = 4$). (M and N) Relative mRNA expression of hypertrophic markers (ANP, BNP, and β -MHC) and fibrosis markers (Col1a, Col3a, and TGF β) quantified by RT-qPCR ($n = 6$). (O to R) Representative images and quantification of PRODH, β -MHC, and ANP protein levels measured by Western blotting ($n = 6$). [Data are shown as means \pm SEM. Two-way analysis of variance (ANOVA) was conducted for the comparisons.]

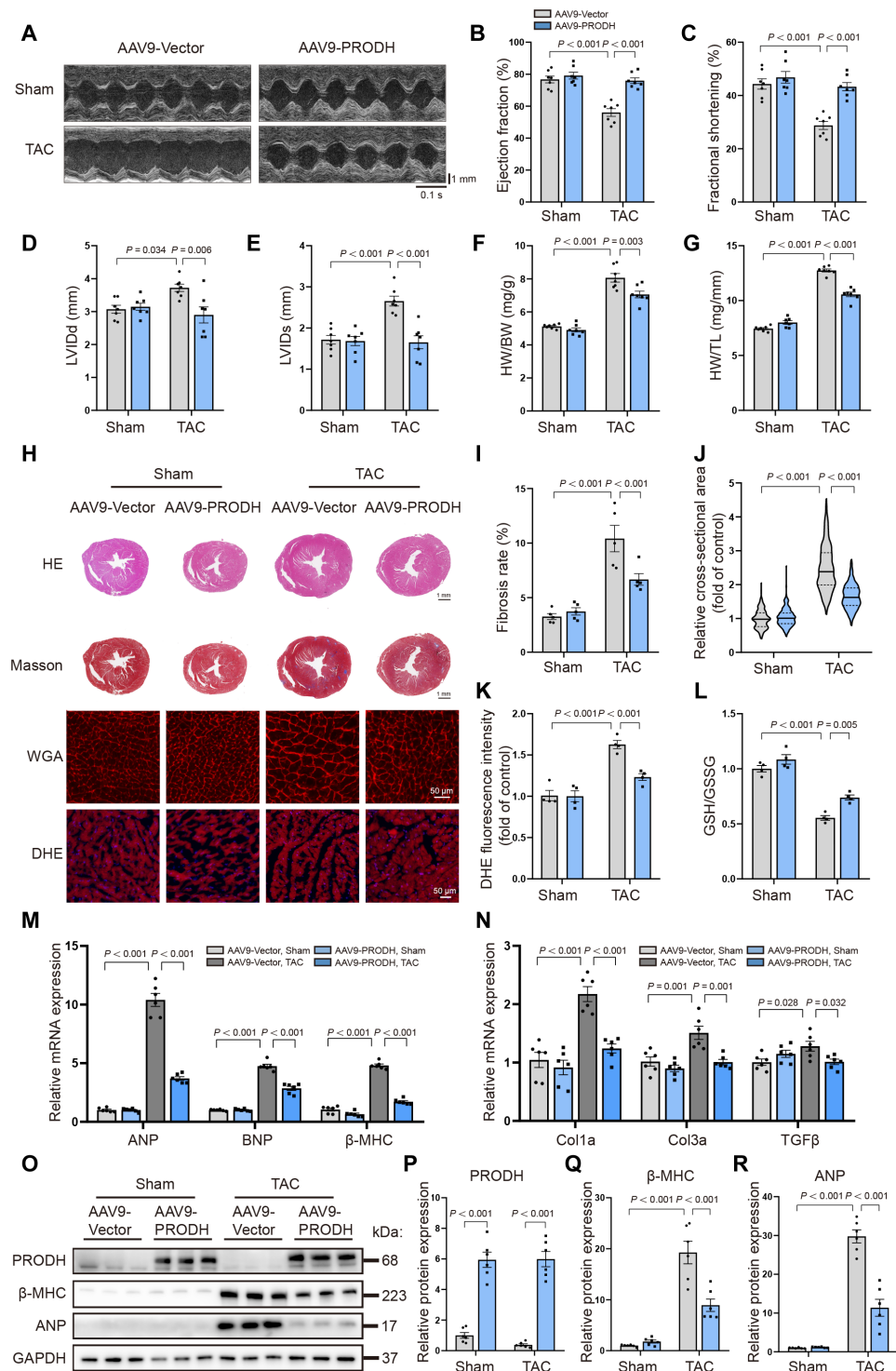


Fig. 3. Cardiac-specific overexpression of PRODH attenuated cardiac remodeling under pressure overload. (A to E) Representative M-mode echocardiography images and quantification of EF and FS, LVlDd, and LVlDs among the AAV9-Vector and AAV9-PRODH mice under either sham or TAC ($n = 7$). (F and G) The ratios of HW/BW and HW/TL ($n = 7$). (H to K) Representative images of H&E staining, Masson's trichrome staining, WGA staining, and DHE and their quantitation results ($n = 5$ for each group of Masson's trichrome staining; $n = 256$ cells for each group of the WGA staining; $n = 4$ for DHE staining). (L) Relative GSH/GSSG ratio of AMCMs isolated from the in vivo experiment ($n = 4$). (M and N) Relative mRNA expression of hypertrophic markers (ANP, BNP, and β -MHC) and fibrosis markers (Col1a, Col3a, and TGF) quantified by RT-qPCR ($n = 6$). (O to R) Representative images and quantification of PRODH, β -MHC, and ANP protein levels measured by Western blotting ($n = 6$). (Data are shown as means \pm SEM. Two-way ANOVA was conducted for the comparisons.)

well-preserved mitochondrial architecture with intact cristae. Conversely, mice treated with AAV9-Vector following TAC surgery exhibited predominantly globular and swollen mitochondria in their cardiac tissues. Notably, AAV9-PRODH mice maintained intact mitochondrial morphology after TAC surgery, suggesting a protective effect of PRODH overexpression on mitochondrial integrity (fig. S5A).

To evaluate whether cardiac-specific PRODH overexpression could reverse established pathological cardiac hypertrophy, we administered AAV9-Vector or AAV9-PRODH 2 weeks after TAC (fig. S6A). Cardiac function, assessed by echocardiography 6 weeks after TAC, revealed that cardiac-specific PRODH overexpression led to improved EF and FS (fig. S6, B to D), along with a reduction in LVDD and LVIDs (fig. S6, E and F). These findings indicated enhanced cardiac performance and reduced ventricular dilation. Consistently, reduced HW/BW and HW/TL ratios in the AAV9-PRODH group suggested a mitigation of ongoing cardiac remodeling (fig. S6, G and H). Collectively, these findings strengthen the protective function of cardiomyocyte PRODH in cardiac remodeling.

PRODH deficiency exacerbated PE-induced cardiomyocyte hypertrophy

Following the revelation of PRODH's protective role against TAC-induced cardiac remodeling from our *in vivo* studies, we turned to an *in vitro* model using NRVMs. NRVMs were stimulated with PE to mimic cardiomyocyte hypertrophy in this study. PRODH expression was silenced in NRVMs using small interfering RNA (siRNA), followed by a 48-hour PE treatment to induce hypertrophy. Consistent with our *in vivo* findings, tetramethylrhodamine isothiocyanate (TRITC)-phalloidin staining revealed that PRODH deficiency notably exacerbated cardiomyocyte hypertrophy *in vitro* (Fig. 4, A and B). This was in line with a marked increase in the mRNA levels of hypertrophic markers ANP, BNP, and β -MHC in PRODH deficiency in cardiomyocytes (Fig. 4C). Similarly, the protein level of β -MHC and ANP was markedly increased upon PRODH loss in cardiomyocytes (Fig. 4, D to G). Moreover, DHE staining revealed that PE treatment increased oxidative stress in cardiomyocytes, which was intensified by PRODH deficiency (Fig. 4, H and I). In addition, the ratio of GSH/GSSG was diminished following PE induction and declined further upon PRODH deficiency (Fig. 4J). These results collectively suggest that PRODH deficiency in cardiomyocytes aggravates cardiomyocyte hypertrophy and oxidative stress.

PRODH overexpression mitigated PE-induced cardiomyocyte hypertrophy

Subsequently, we studied the role of PRODH overexpression in NRVMs on hypertrophy and oxidative damage *in vitro*. Therefore, an adenovirus 4 (ADV4)-mediated PRODH overexpression adenovirus (Ad-PRODH) was added to NRVMs before a 48-hour PE stimulation. Notably, TRITC-phalloidin staining revealed that PRODH overexpression in NRVMs led to a noticeable reduction in the cardiomyocyte surface area after PE exposure (Fig. 5, A and B). This reduction was paralleled by a marked decrease in mRNA expression of hypertrophic markers ANP, BNP, and β -MHC upon PE treatment (Fig. 5C). Consistently, the protein levels of β -MHC and ANP were also reduced in PRODH-overexpressed cardiomyocytes (Fig. 5, D to G). In alignment with these observations, DHE staining, the indicator of oxidative stress of NRVMs, showed a notably protective effect of PRODH from oxidative damage after PE stimulation (Fig. 5, H

and I). The increased GSH/GSSG ratio also revealed that PRODH overexpression notably up-regulated the antioxidant ability of cardiomyocytes (Fig. 5J). In summary, these results reinforce the conclusion that PRODH overexpression in cardiomyocytes protects them against hypertrophy and oxidative stress.

PRODH overexpression effectively reprogrammed cardiac metabolic shifts induced by TAC

To investigate the cardioprotective effects of PRODH overexpression in the context of pressure overload-induced cardiac remodeling, we simultaneously conducted RNA-seq on isolated AMCMs and cardiac tissue of the mice subjected to either TAC or sham surgery with cardiac-specific PRODH overexpression, as shown in Fig. 6 and fig. S7, respectively, and similar observations were obtained. We first conducted differential gene analysis, confirming the decrease in PRODH levels in cardiomyocytes and cardiac tissues after TAC surgery and its up-regulation following PRODH overexpression (Fig. 6, A and B, and fig. S7, A and B). The control group, treated with AAV9-Vector, exhibited 3768 down-regulated genes and 3867 up-regulated genes among AMCMs after TAC compared with the sham group. In contrast, hearts overexpressing PRODH showed 2956 up-regulated genes and 3339 down-regulated genes among AMCMs following TAC compared to AAV9-Vector controls (Fig. 6, C and D). For the results from RNA-seq of cardiac tissues, 3055 down-regulated genes and 2297 up-regulated genes were observed for the comparison between the TAC group and the sham group among the mice receiving AAV9-Vector. Overexpression of PRODH showed 3006 up-regulated genes and 2248 down-regulated genes following TAC compared to AAV9-Vector controls (fig. S7, C and D). A detailed study of these gene expression alterations revealed that PRODH overexpression counteracted the TAC-induced down-regulation of 1129 genes and the up-regulation of 1345 genes among AMCMs and the down-regulation of 1093 genes and the up-regulation of 770 genes among cardiac tissues. Furthermore, we performed Kyoto Encyclopedia of Genes and Genomes (KEGG) enrichment analysis of these counteracted gene by overexpression of PRODH. The results indicated that TAC prompted notable alterations in cardiac metabolism, including reductions in valine, leucine, and isoleucine degradation; carbon metabolism; propanoate metabolism; and citrate cycle (TCA cycle) among AMCMs (Fig. 6E). Notably, these metabolic perturbations were largely reversed by PRODH overexpression. In addition, PRODH overexpression was found to mitigate the enhanced expression of several key biological processes related to cardiac modeling, such as focal adhesion, extracellular matrix (ECM)-receptor interaction, and phagosome (Fig. 6F). These results suggested that PRODH had a crucial role in reducing structural remodeling upon TAC. Similarly, the results from cardiac tissue indicated that overexpression of PRODH reversed the inhibited cardiac metabolism induced by TAC, including carbon metabolism, TCA cycle, 2-oxocarboxylic acid metabolism, and valine, leucine, and isoleucine degradation (fig. S7E). It also mitigated the enhanced expression of several cardiomyopathic pathways after TAC, such as dilated cardiomyopathy, HCM, lysosome, and protein digestion and absorption (fig. S7F).

The replenishment of TCA intermediates in cardiomyocytes is crucial for maintaining cardiac function after TAC surgery. Previous studies have established that proline can be metabolically converted into glutamate, which then deaminates to α -ketoglutarate and enters the TCA cycle (16, 18). Thus, we further explored the enrichment

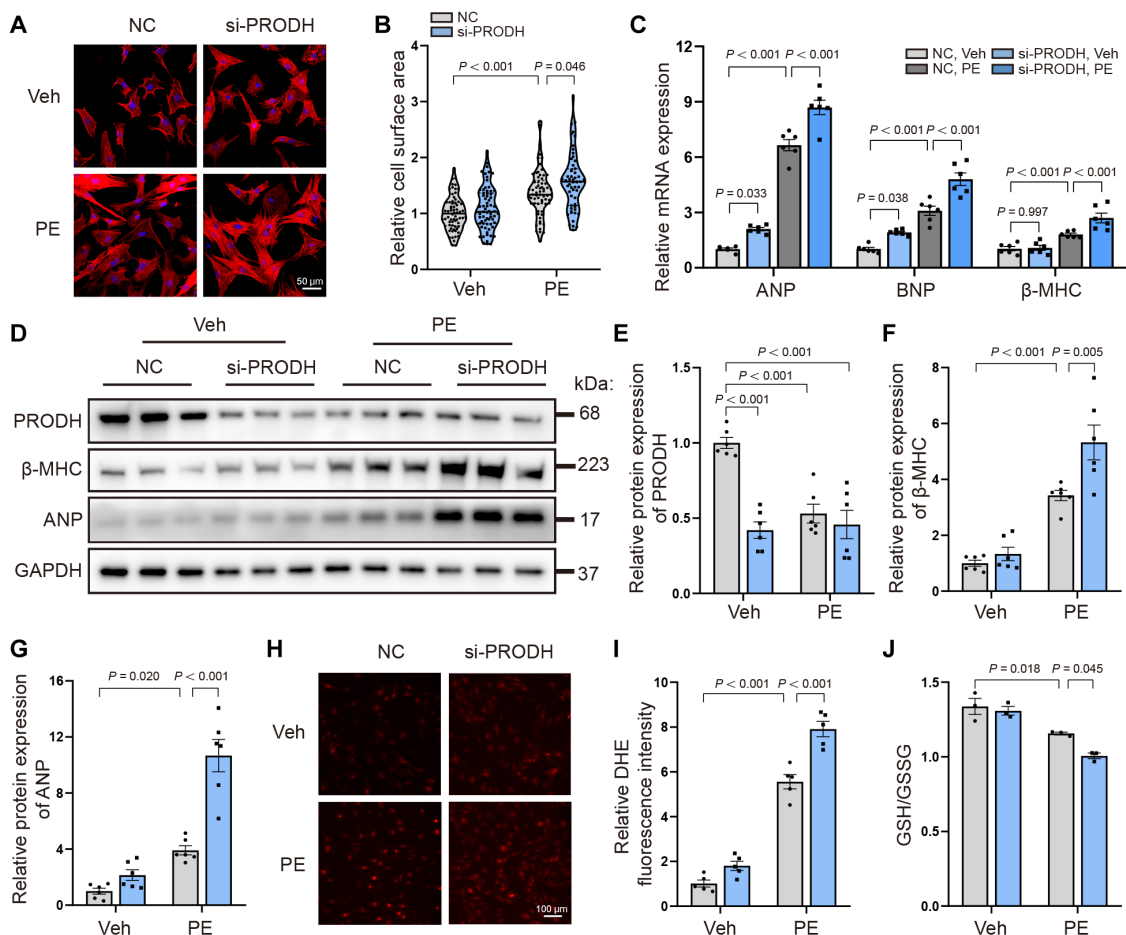


Fig. 4. Silencing PRODHD aggravated PE-stimulated cardiomyocyte hypertrophy in vitro. (A and B) Representative images and quantification of cultured NRVMs stained with TRITC-labeled phalloidin (red) and nuclei (blue) ($n = 66$ for NC, Veh; $n = 67$ for si-PRODHD, Veh; $n = 65$ for NC, PE; $n = 55$ for si-PRODHD, PE). (C) Relative mRNA expression of ANP, BNP, and β -MHC quantified by RT-qPCR ($n = 6$). (D to G) Representative images and quantification of PRODHD, β -MHC, and ANP protein levels measured by Western blotting ($n = 6$). (H and I) Representative images and quantification of cultured NRVMs stained with DHE (red) ($n = 5$). (J) Quantification of GSH/GSSG after silencing PRODHD and/or stimulated with PE ($n = 3$). (Data are shown as means \pm SEM. Two-way ANOVA was conducted for the comparisons.)

analysis of TCA cycle, a key metabolic process of interest to us, of two individual sequencing experiments. The results revealed by gene set enrichment analysis (GSEA) confirmed that the TCA cycle was notably enriched in AMCMs and cardiac tissues after PRODHD overexpression (Fig. 6G and fig. S7G). In addition, we constructed a heatmap based on two RNA-seq data to present the expression profiles of genes in proline catabolism and anabolism, alongside those in the TCA cycle (Fig. 6H and fig. S7H). Our findings from two datasets both indicated a notable down-regulation of proline catabolism-related genes, including *Prodh*, *pyrroline-5-carboxylate dehydrogenase (P5cdh)*, *ornithine aminotransferase (Oat)*, and *glutamate dehydrogenase 1 (Glu1)* following TAC, which was restored upon PRODHD overexpression. Conversely, genes in proline synthesis, such as *pyrroline-5-carboxylate reductase (Pycr1)* and *pyrroline-5-carboxylate synthase (P5cs)*, displayed an up-regulation after TAC, which was reversed by PRODHD overexpression. Furthermore, we observed that genes in the TCA cycle were substantially down-regulated after TAC, but their expression levels were substantially restored by PRODHD overexpression.

After elucidating the changes in proline metabolism and the TCA cycle through RNA-seq, we further conducted metabolite profiling of

cardiac tissue after TAC via untargeted metabolomics. The results showed that proline levels in the TAC group among the AAV9-Vector mice were markedly higher than those in the sham group, accompanied by a decrease in levels of TCA metabolic intermediates such as succinate, malate, and citrate (Fig. 6, I to L). Conversely, in AAV9-PRODHD mice with TAC surgery, the proline levels were noticeably lower compared with those in AAV9-Vector mice, but the levels of TCA intermediates were prominently elevated. This result suggested that overexpression of PRODHD not only enhanced the utilization of proline among cardiomyocytes but also promoted the levels of TCA cycle intermediates. Collectively, these findings imply that TAC suppresses proline catabolism and the subsequent TCA cycle, while PRODHD overexpression in cardiomyocytes counteracts these effects and restores normal TCA cycle by reprogramming proline metabolism.

The metabolic reprogramming induced by PRODHD overexpression restored the TCA cycle in cardiomyocyte hypertrophy

We primarily compared the metabolic changes induced by PE stimulation and the metabolic effects of PRODHD overexpression or

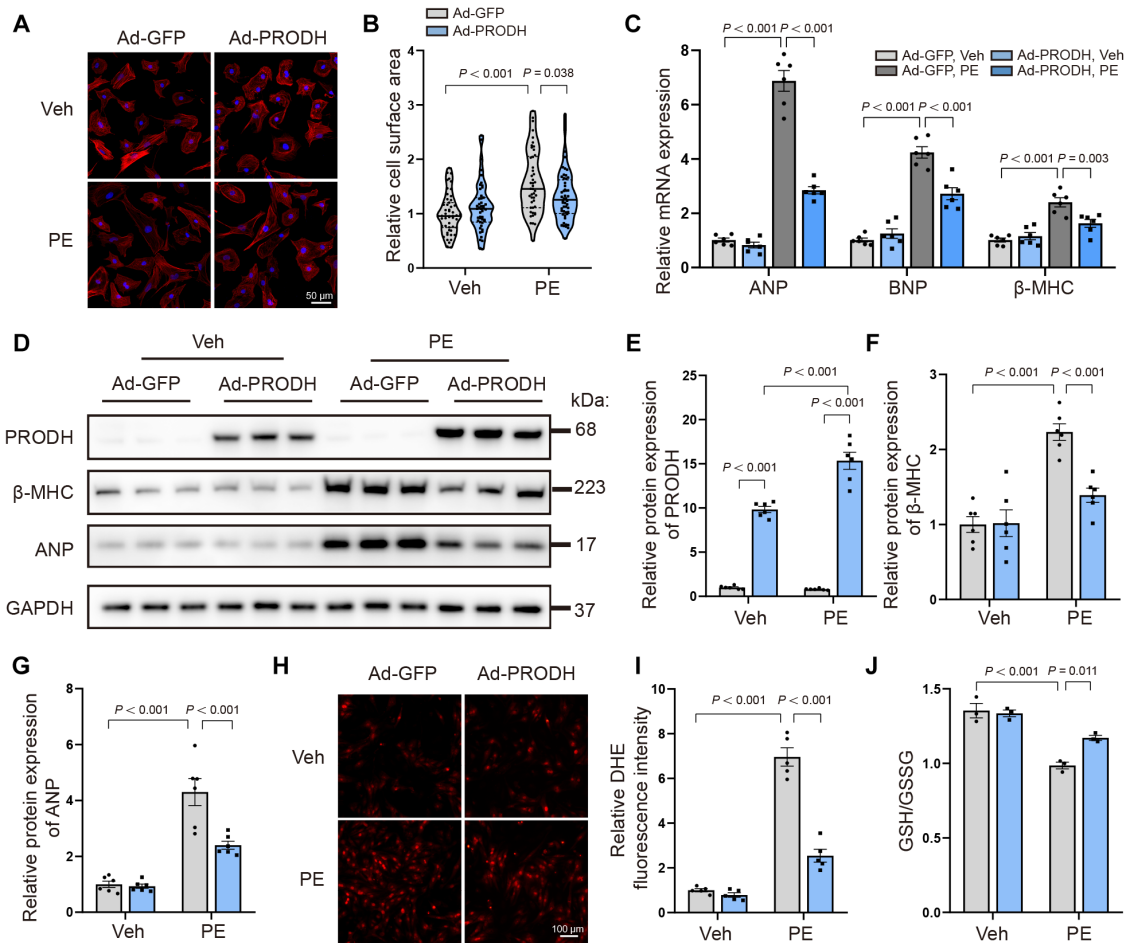


Fig. 5. Overexpression of PRODH attenuated PE-stimulated cardiomyocyte hypertrophy in vitro. (A and B) Representative images and quantification of cultured NRVMs stained with TRITC-labeled phalloidin (red) and nuclei (blue) ($n = 51$ for Ad-GFP, Veh; $n = 47$ for Ad-PRODH, Veh; $n = 46$ for Ad-GFP, PE; $n = 52$ for Ad-PRODH, PE). (C) Relative mRNA expression of ANP, BNP, and β -MHC quantified by RT-qPCR ($n = 6$). (D to G) The representative images and quantification of PRODH, β -MHC, and ANP protein levels measured by Western blotting ($n = 6$). (H and I) Representative images and quantification of cultured NRVMs stained with DHE (red) ($n = 5$). (J) Quantification of GSH/GSSG after silencing PRODH and/or stimulated with PE ($n = 3$). (Data are shown as means \pm SEM. Two-way ANOVA was conducted for the comparisons.)

knockdown on PE-induced cardiomyocyte hypertrophy. Orthogonal partial least squares discriminant analysis (OPLS-DA) revealed distinct metabolic patterns among cells subjected to different treatments (Fig. 7, A and B, and fig. S8, A and B). In the PRODH overexpression experiment, PE stimulation modulated a subset of 33 metabolites in the adenovirus–green fluorescent protein (Ad-GFP) group, with 17 up-regulated metabolites and 16 down-regulated metabolites from a pool of 257 analyzed metabolites, while PRODH overexpression up-regulated 20 metabolites and down-regulated 16 metabolites compared to the PE-stimulated group with negative virus (Fig. 7C). In the PRODH knockdown experiment, PE stimulation up-regulated 26 metabolites and down-regulated 14 metabolites out of 250 detected metabolites, whereas PRODH knockdown resulted in the up-regulation of 11 metabolites and down-regulation of 28 metabolites (fig. S8C). Volcano plots depicted the most profoundly altered metabolites (Fig. 7, D and E, and fig. S8, D and E).

The results of Z -score normalization intuitively illustrated the changes of differentially expressed metabolites (DEMs) after various treatments (Fig. 7, F and G, and fig. S8, F and G). Both experiments consistently showed elevated levels of proline and TCA cycle

intermediates such as citrate, succinate, and fumarate, along with increased adenosine triphosphate (ATP) levels. PE stimulation also decreased reduced glutathione, accompanied by elevated oxidized glutathione levels. Overexpression of PRODH decreased proline levels and further up-regulated TCA cycle intermediates and ATP levels, reversing the decreased glutathione and increased oxidized glutathione levels. Knockdown of PRODH exhibited opposite effects.

KEGG pathway analysis further supported our observations. Enrichment analysis of DEMs revealed that PE stimulation up-regulated several key metabolic pathways in cardiomyocytes, such as central carbon metabolism in cancer, the glucagon signaling pathway, and the TCA cycle (Fig. 7H and fig. S8H). PRODH overexpression induced changes in pathways including central carbon metabolism in cancer, the GABAergic synapse, and the TCA cycle (Fig. 7I), while PRODH knockdown mainly affected processes such as central carbon metabolism in cancer, protein digestion and absorption, aminoacyl-transfer RNA biosynthesis, and the TCA cycle (fig. S8I). Together, these results fully illustrated the metabolic differences in hypertrophic cardiomyocytes and the metabolic reprogramming induced by PRODH regulation. These results together

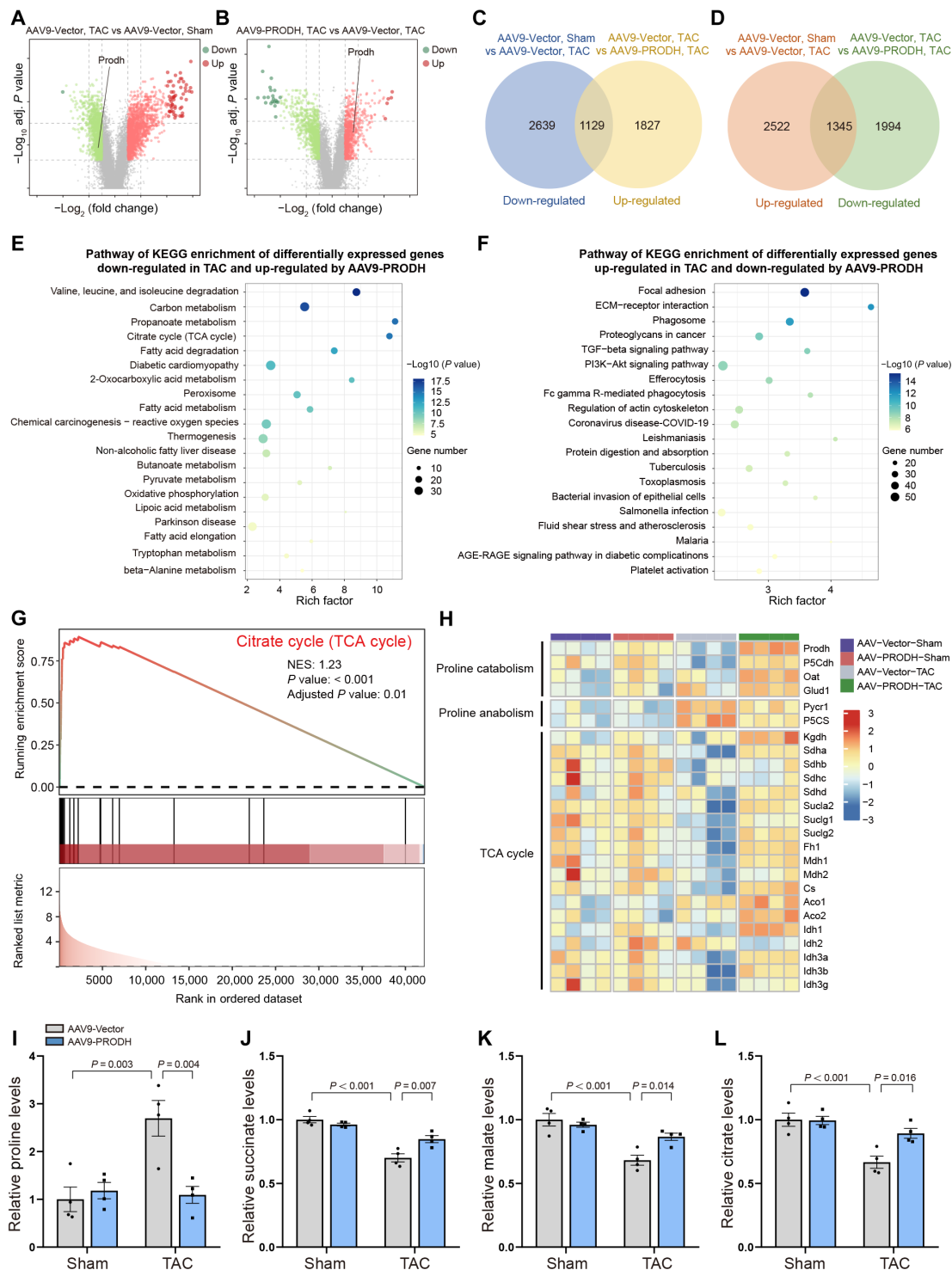


Fig. 6. PRODH overexpression effectively reprogrammed cardiac metabolic shifts induced by TAC. (A and B) Volcano plot of two comparisons from the RNA-seq data of AMCMs: AAV9-Vector, TAC versus AAV9-Vector, sham and AAV9-PRODH, TAC versus AAV9-Vector, TAC. (C and D) Venn diagram of differentially expressed genes (DEGs) down-regulated by TAC surgery and up-regulated by PRODH overexpression and up-regulated by TAC surgery and down-regulated by PRODH overexpression, respectively. (E and F) KEGG pathway analysis of the DEGs down-regulated by TAC surgery and rescued by overexpression of PRODH and up-regulated by TAC surgery and inhibited by overexpression of PRODH, respectively. (G) GSEA of the dataset of the citrate cycle (TCA cycle). (H) Heatmap of the expression profile of proline catabolism, proline anabolism, and TCA cycle acquired by the RNA-seq data ($n = 4$ mice per group). (I to L) Relative proline and TCA intermediate levels of cardiac tissues after TAC surgery and PRODH overexpression ($n = 4$). (Data are shown as means \pm SEM. Two-way ANOVA was conducted for the comparisons.)

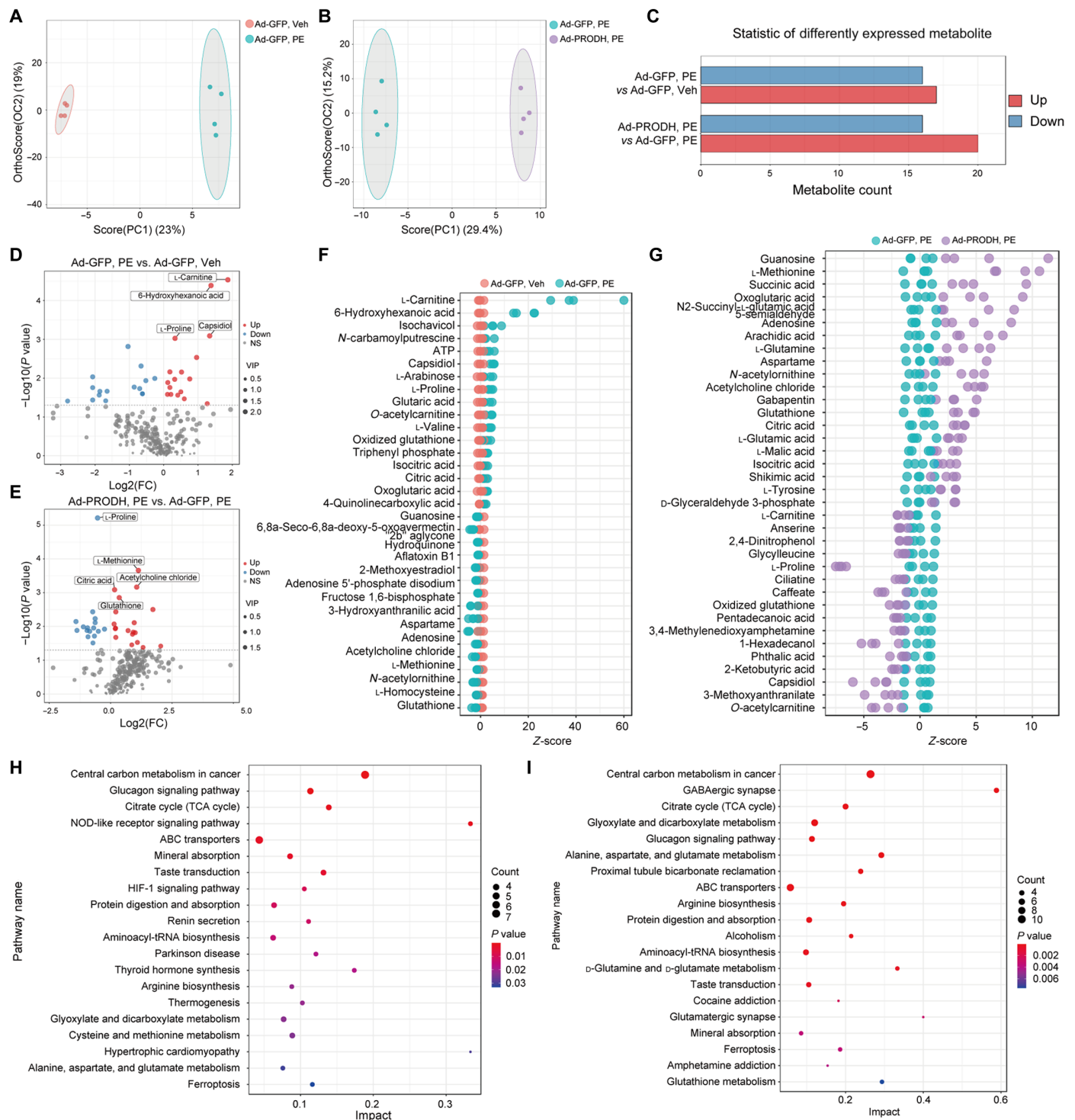


Fig. 7. The metabolic reprogramming induced by PRODH overexpression restored the TCA cycle in cardiomyocyte hypertrophy. (A and B) OPLS-DA of metabolome data for the comparison between the Ad-GFP, Veh group and the Ad-GFP, PE group, and between the Ad-GFP, PE group and the Ad-PRODH, PE group, respectively. (C) Statistic of differently expressed metabolite of two comparisons: Ad-GFP, Veh versus Ad-GFP, PE and Ad-GFP, PE versus Ad-PRODH, PE, respectively. (D and E) Volcano plot of two comparisons. (F and G) Z-score plot showing the changes of DEMs from two comparisons. (H and I) KEGG pathway analysis of the DEMs of two comparisons ($n = 4$ for each group).

highlight the critical role of PRODH in modulating the TCA cycle, oxygen metabolism, and glutathione homeostasis.

PRODH overexpression replenishes mitochondrial respiration and TCA cycle in cardiomyocytes

Next, we asked the effect of PRODH overexpression on mitochondrial respiration and TCA cycle restoration. To address this, we measured oxygen consumption rate (OCR) using Seahorse flux analysis and found that PRODH up-regulated oxygen consumption in cardiomyocytes, regardless of PE stimulation (Fig. 8A). This increase in OCR was in agreement with the observed rise in basal OCR, ATP-linked OCR, and maximal OCR (Fig. 8, B to D). Notably, the increase in ATP-linked OCR corresponded with a noticeable elevation in ATP levels in PRODH-overexpressed cardiomyocytes (Fig. 8E).

To determine whether proline catabolism via PRODH could replenish TCA cycle intermediates, we conducted isotope labeling experiments using L-proline- ^{13}C , ^{15}N to trace the integration of proline into the TCA cycle (Fig. 8F). Overexpression of PRODH in

cardiomyocytes channeled proline into the TCA cycle, resulting in enhanced α -ketoglutarate (α -KG), succinate (Suc), fumarate (Fum), malate (Mal), and citric acid (Cit) derived from proline, independent of PE stimulation (Fig. 8, G to K). These findings suggest that, by promoting the anaplerotic use of proline, PRODH overexpression effectively restores the TCA cycle, thereby enhancing mitochondrial respiration in hypertrophic cardiomyocytes.

DISCUSSION

In this study, we mainly investigated the alterations of proline metabolism during pressure overload-induced cardiac remodeling and further determined the role of PRODH in regulating cardiac function and metabolic remodeling of cardiomyocytes. We observed a notable down-regulation of PRODH in the hearts of mice after TAC surgery, indicating impaired proline metabolism during pressure-induced cardiac remodeling. Subsequently, we found that cardiac-specific PRODH knockout mice showed deteriorated cardiac

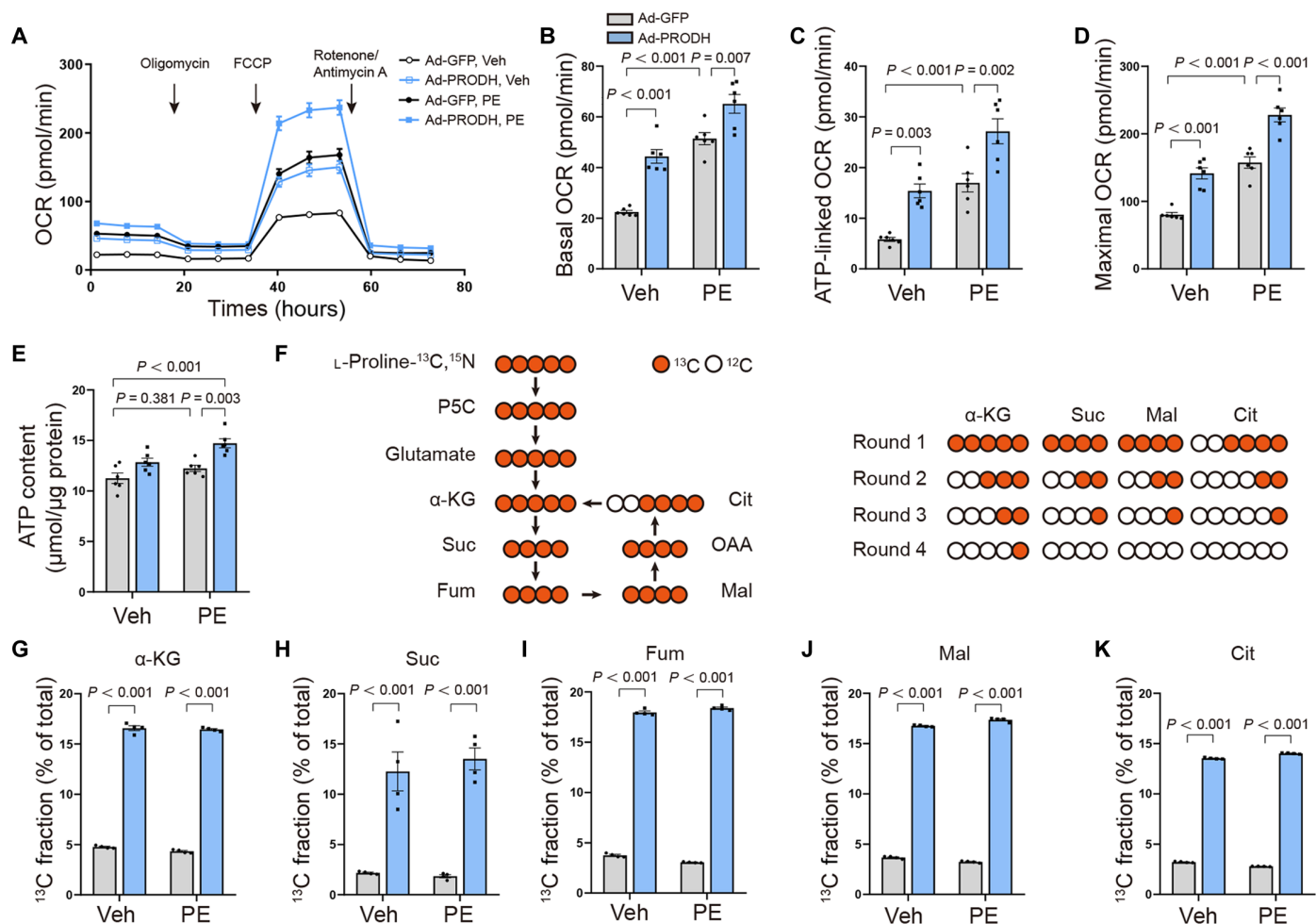


Fig. 8. PRODH overexpression replenishes mitochondrial respiration and TCA cycle in cardiomyocytes. (A) Mitochondrial respiration of NRVMs was determined by measuring OCR. (B to D) Basal, ATP-linked, and maximal OCRs of NRVMs measured by Seahorse ($n = 6$). (E) ATP content of NRVMs receiving different treatments measured by the commercial kit ($n = 6$). (F) Schematic of ^{13}C -labeling pattern in NRVMs. After entering the TCA cycle, ^{13}C -labeled L-proline was catabolized mostly into M5/M4 metabolites in the first round (round 1) of the TCA cycle, M3/M2 in round 2, M2/1 in round 3, and M1/0 in round 4. (G to K) Incorporation of ^{13}C -proline into the tricarboxylic acid cycle, as revealed by the ^{13}C fraction of total C of α -KG, Suc, Fum, Mal, and Cit ($n = 4$). α -KG, α -ketoglutarate; Suc, succinate; Fum, fumarate; Mal, malate; Cit, Citrate. (Data are shown as means \pm SEM. Two-way ANOVA was conducted for the comparisons.)

function after TAC, whereas PRODH overexpression in cardiomyocytes appeared cardioprotective. Further *in vitro* analyses revealed that PRODH overexpression in NRVMs not only increased TCA cycle metabolites and ATP production but also reduced oxidative stress by modulating glutathione synthesis and enhancing the GSH/GSSG ratio, thus boosting antioxidant defense in cardiomyocytes (Fig. 9).

In response to persistent hemodynamic stress from pressure overload, the heart undergoes myocardial remodeling, namely, cardiomyocyte hypertrophy, to adapt to the increased workload (22). Enlarged cardiomyocytes necessitate elevated energy consumption for cell growth and contractile function, leading to a profound energy shortage in the end (23). Therefore, the cardiomyocytes undergo profound changes to meet the demand of energy during the myocardial hypertrophy and its progression to HF. Cardiomyocytes primarily depend on fatty acid oxidation to meet the high energy demand of the heart as a biology pump under physiological conditions. Of note, cardiac remodeling triggers a metabolic shift in substrate utilization, characterized by reduced ATP production from fatty acids and increased dependence on glycolysis and ketone body oxidation for compensation of energy (8). However, this compensation is limited because glycolysis is less efficient at ATP generation. The heightened glycolytic activity cannot fully mitigate the energy shortfall or restore cardiac function in HF. Therefore, modulating cardiac energy metabolism to enhance ATP synthesis in cardiomyocytes can remarkably preserve cardiac function.

In addition to increased glycolysis and ketone utilization, the reprogramming of amino acid metabolism also exerts a pivotal role in redox homeostasis and cellular growth of cardiomyocytes during pressure overload-induced myocardial remodeling (24). Sun *et al.* (25) reported a notable inhibition of branched-chain amino acid (BCAA) catabolic gene expression in HF. The defect in BCAA catabolic enzymes promoted HF as the up-regulation of BCAAs directly inhibited mitochondrial respiration, leading to superoxide production. In addition, Ritterhoff *et al.* (26) identified aspartate as a crucial amino acid contributing to myocardial hypertrophy. Up-regulation of fatty acid oxidation by deletion of acetyl-CoA-carboxylase 2 inhibited glucose-derived aspartate synthesis, thereby suppressing myocardial hypertrophy. Currently, the role of other amino acids in pathological myocardial remodeling remains incompletely elucidated.

PRODH is a mitochondrial enzyme that plays a pivotal role in cellular homeostasis by regulating proline metabolism. It catalyzes the transformation of proline into glutamate, which can either be used in the TCA cycle for energy production or serve as a precursor for other amino acids (18). Recent research has expanded our understanding of PRODH, highlighting its involvement in various cellular processes such as energy metabolism, apoptosis, and the oxidative stress response (13). In our study, we observed a notable down-regulation of PRODH expression in cardiac tissues after TAC surgery and in hypertrophic cardiomyocytes stimulated by PE, with a corresponding reduction in its activity demonstrated in *in vivo* experiments. These findings suggest that the catabolic metabolism of proline is suppressed during cardiac remodeling. The underlying cause of PRODH down-regulation in cardiomyocytes remains unclear. However, we observed partial restoration of PRODH expression in mouse cardiac tissues treated with rapamycin after TAC surgery. Previous studies have identified mTOR as an inhibitory regulator of PRODH (15, 17), and its activation during TAC-induced myocardial remodeling to promote compensatory cardiomyocyte hypertrophy is well established (20, 21). mTOR senses the cellular nutrient and energy status and enhances processes such as glycolysis, protein, lipid, and nucleotide biosynthesis, thereby systematically altering cardiomyocyte synthesis and degradation metabolism (27). Hence, we speculate that the expression of PRODH may be inhibited by activation of the mTOR signaling pathway during the cardiac remodeling.

In the context of cardiovascular diseases, the significance of PRODH has been progressively recognized. Proline metabolism was initially identified as a differential metabolite in HF (9, 19), yet research is required to elucidate the underlying mechanisms. Moreira *et al.* (28) first reported a notable down-regulation of PRODH expression in rat myocardium following myocardial infarction. They found that physical exercise could reverse this down-regulation and concurrently enhance cardiac function. However, this study did not perform PRODH expression *in vivo* experiments to explore its protective effects. By using induced pluripotent stem cell-derived cardiomyocytes, they found that PRODH knockdown increased BNP expression, while PRODH overexpression up-regulated oxidative phosphorylation in cardiomyocytes. In addition, PRODH knockdown resulted in reduced mitochondrial OCR and decreased

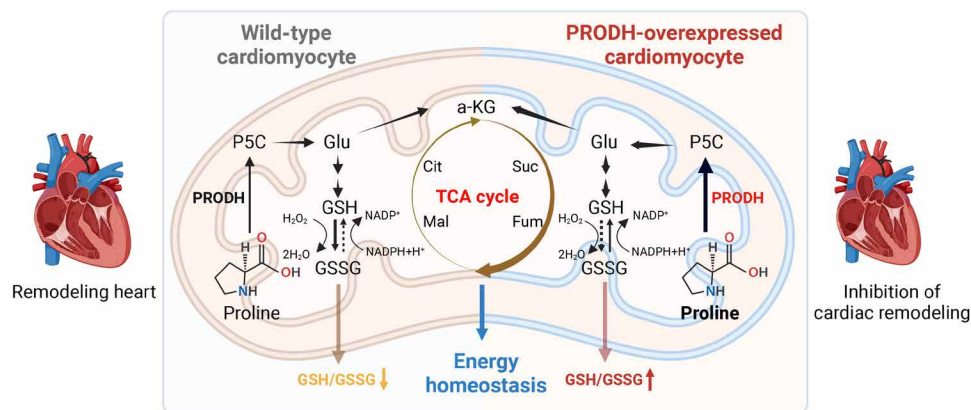


Fig. 9. Schematic illustration depicting the impact of PRODH overexpression in the inhibition of cardiac remodeling. The wild-type mice exhibit deficiencies in energy homeostasis along with decreased GSH/GSSG levels following TAC surgery. Cardiomyocytes overexpressing PRODH facilitate the utilization of proline, promoting its conversion into the TCA cycle and up-regulating GSH/GSSG levels.

ATP synthesis, whereas PRODH overexpression up-regulated mitochondrial OCR and ATP production. Our cellular observations are aligned with their research. In addition, in our *in vitro* experiments, we confirmed that PRODH overexpression mildly increased mitochondrial OCR and ATP production at baseline. Meanwhile, PRODH overexpression markedly enhanced ATP supply by PE stimulation. Our RNA-seq and metabolomic studies, supported by isotopic labeling metabolic flux assays, confirm that PRODH promoted mitochondrial energy supply by augmenting the production of TCA intermediates.

Furthermore, we substantiated the above findings by conducting additional metabolic profiling of *in vivo* experiments. We initially investigated the fate of proline in cardiac remodeling and found a remarkable up-regulation of proline levels after TAC surgery, consistent with the finding of down-regulation of PRODH expression after TAC surgery. Cardiac-specific overexpression of PRODH reversed the elevation of proline after TAC, indicating that PRODH overexpression promoted cardiac proline utilization. Subsequently, we also observed a notable down-regulation of TCA cycle intermediates in mouse cardiac tissues 4 weeks after TAC surgery, which was reversed by PRODH overexpression. These findings align with our RNA-seq analysis of primary cardiomyocytes isolated after TAC surgery, demonstrating that PRODH up-regulates the decreased catabolic enzyme of proline and TCA cycle-related enzymes during cardiac remodeling. These conclusions further confirm the critical regulatory role of PRODH in proline metabolism and the TCA cycle, suggesting a therapeutic potential for addressing the energy insufficiency in HF.

In the failing heart, elevated levels of reactive oxygen species (ROS) lead to mitochondrial DNA damage, antioxidant depletion, and reduced mitochondrial ATP production, aggravating the cardiac remodeling eventually (29, 30). PRODH has been previously reported to modulate mitochondrial function by regulating ROS and maintaining mitochondrial integrity (31). It has been found that PRODH expression is up-regulated in response to oxidative stress to maintain cellular redox balance (32). Our previous study has proven that PRODH exerted a protective effect against oxidative stress damage through the utilization of proline in myocardial infarction (33). Specifically, dietary proline supplementation could profoundly mitigate oxidative stress damage and reduce myocardial apoptosis after myocardial infarction. Consistent with these findings, *in vitro* experiments with cardiomyocytes subjected to hypoxia further corroborated the same conclusion (34). The findings from this study align with these observations above. Specifically, in PRODH cKO mice after TAC surgery, a marked exacerbation of oxidative stress damage was observed, while PRODH-overexpressed mice exhibited attenuated oxidative stress induced by pressure overload. Similar results were found in the NRVMs stimulated by PE. The administration of the antioxidant NAC partially improved the deteriorated cardiac function in cKO mice after TAC, accompanied by a decrease in heart weight. This finding demonstrated that the exacerbated oxidative stress in cKO mice is as a crucial contributor of the deterioration of cardiac function.

Our results also hinted that PRODH participated in glutathione redox homeostasis by regulating the GSH/GSSG ratio. Overexpression of PRODH was found to elevate the GSH/GSSG ratio, while down-regulation of PRODH inhibited the GSH/GSSG ratio in both *in vivo* and *in vitro* experiments. These results provide insight into the role of PRODH in enhancing cellular antioxidant capacity.

In our mechanistic investigations, we observed that, despite the lack of up-regulation in the expression of the key enzyme GCLC involved in glutathione synthesis, overexpression of PRODH led to an increase in the expression of GSR. This phenomenon suggests a potential facilitation of the conversion of GSSG to GSH within cardiomyocytes.

This study illustrated the protective role of PRODH expression in cardiomyocytes during cardiac remodeling and elucidates its underlying mechanisms. However, there are still some limitations that need to be addressed. First, evaluations of cardiomyocyte function, especially mitochondrial respiratory function and isotope labeling experiments, were conducted *in vitro*. Performing an *in vivo* experiment would further solidify these findings. Second, while our experiments have demonstrated a correlation between the PRODH expression and mTOR signaling pathway, further experiments are still needed to explore whether there is a causal relationship, which would help explain why PRODH is down-regulated after TAC. Lastly, additional research elucidating the direct regulatory effects of PRODH on GSR expression would further deepen our understanding of how PRODH maintains glutathione homeostasis.

In conclusion, this study reveals the reprogramming of proline metabolism during cardiac remodeling and its potential therapeutic implications. PRODH is shown to alleviate cardiac remodeling by reestablishing energy production through the enhanced TCA cycle and the improved antioxidant capacity of cardiomyocytes. These findings highlight the potential of targeting proline metabolic pathways as a treatment strategy for cardiac remodeling caused by pressure overload.

MATERIALS AND METHODS

Experimental animals and experimental protocols

All animal experiments followed the Institutional Animal Care Guidelines and were approved by the Animal Experimentation Ethics Committee of Zhejiang University. The 8- to 10-week-old wild-type C57BL/6 male mice and 1- to 3-day-old neonatal Sprague-Dawley (SD) rats were purchased from the Vital River Laboratory Animal Technology Co., Ltd. (Beijing, China). The cardiac-specific conditional PRODH knockout mice were generated by Cyagen Biosciences (Guangzhou, China). In brief, the mouse *Prodh* gene contains 13 exons; exon 3 to 8 of *Prodh* was chosen for targeting using a CRISPR-Cas9-mediated genome-editing approach. The floxed mice were crossed with Myh6-iCre mice to generate the cardiac-specific PRODH cKO mice. The C57BL/6 mice mentioned above were maintained in a pathogen-free animal house with a 12-hour light/dark cycle and constant temperature. All animal experiments were approved by the Institutional Animal Care and the Use Committee of Zhejiang University.

For the investigation of the relationship between mTOR and PRODH, wild-type mice after TAC were randomly divided into two groups. They were intraperitoneally injected with rapamycin at a dose of 2 mg/kg per day or an equivalent volume of saline. After 28 days, mouse cardiac tissues were obtained for relevant examinations (35). To investigate whether NAC can restore the impaired cardiac function in cKO mice following TAC surgery, both *f/f* and cKO mice were randomly divided into two groups after TAC operation. They were administered either 500 mg/kg per day of NAC or saline orally for 28 days, followed by relevant experimental assessments (36).

TAC model

To build a model of pressure overload–induced cardiac hypertrophy, TAC surgery was performed among C57BL/6 male mice of 8 to 10 weeks old. Briefly, the mice were first anesthetized with 0.3% sodium pentobarbital (25 ml/kg, intraperitoneally). A minimally invasive surgical incision was conducted on the upper edge of the second rib in the left chest after the mouse had no toe-pinch reflex. The thoracic aorta was then identified with the help of a stereomicroscope. A 27-gauge needle and 6-0 silk sutures were then used to ligate the thoracic aorta between the innominate and left carotid arteries. When the needle was removed, a region of stenosis among the thoracic aorta was successfully presented. Lastly, the incision was closed by 4-0 silk sutures. The mice were lastly placed under a heat lamp until anesthesia recovery. Efforts were made to minimize the suffering of the mice in all experiments.

Echocardiography

Echocardiography was performed by the Vevo 1100 system (Visual-Sonics Inc., Toronto, Canada) equipped with a 30-MHz ultrasound transducer as previously described (37). The long-axis view of M-mode images was captured to analyze various parameters, including EF, FS, LVIDd, and LVIDs.

AAV9 delivery

For cardiac-specific exogenous expression of PRODH, recombinant AAV9 overexpressing a full-length mouse PRODH cDNA was constructed into a plasmid containing a chicken troponin T promoter, obtained from Hanheng Biotechnology (Shanghai, China). AAV9-Vector was produced as a negative control. The viruses were delivered to mice with a dose of 1×10^{11} virus particles (vg) via tail injection before or after the TAC surgery according to the experimental design.

Histology analysis

The hearts of mice after TAC surgery were harvested and immediately fixed in 4% paraformaldehyde (PFA) at room temperature for 24 hours. Subsequently, the hearts were embedded in paraffin and cut into 5- μ m-thick sections. H&E staining and Masson's trichrome staining were performed to observe the gross morphology and fibrosis areas of the hearts following standard procedures, respectively.

Isolation of NRVMs and cell culture

Neonatal SD rats aged 1 to 3 days old were used to isolate NRVMs. First, the hearts removed from the neonatal rats were cut into 1- to 2-mm pieces and washed twice with cold phosphate-buffered saline (PBS). The tissue was then digested by the mixture of 0.04% Collagen II and 0.06% trypsin 8 to 10 times for 8 min each. The cells collected from each digestion were temporarily kept on ice. After the digestion, the cells were collected by centrifugation at 1000 rpm for 5 min. The cells were then resuspended by red blood cell lysis buffer (Solarbio Science and Technology Co., Ltd., Beijing, China) to remove the red blood cells. The myofibroblasts were separated by the differential adhesion method. The myocytes were plated in gelatin-coated plates at a density of 5×10^5 cells/ml by Dulbecco's modified Eagle's medium (DMEM) with 10% fetal bovine serum and bromodeoxyuridine (100 μ M). After 24 hours, the myocytes were then cultured by the serum-free DMEM for at least 12 hours before further experiments.

Isolation of AMCMs

The isolation of AMCMs was conducted using the Langendorff isolated heart perfusion system, closely adhering to methodologies delineated in a prior publication (38). Initially, the perfusion buffer, Krebs-bicarbonate solution, stopping buffer, and myocyte digestion buffer were prepared, which are listed in tables S1 to S4. An adult mouse heart was then excised and immediately placed in a 60-mm dish filled with perfusion buffer to ensure complete expulsion of blood. The aorta was identified, clamped with forceps, and mounted onto a Langendorff needle in a precise manner. Upon establishment of this setup, the perfusion was initiated with the pump activated at a flow rate of 3 to 4 ml/min. Following a period of 5 min, the enzyme solution was perfused at an adjusted flow rate of 5 to 6 ml/min. After 15 min of enzymatic perfusion, observations indicated that the heart had swollen and turned slightly pale, signifying complete digestion. The heart was then transferred to a fresh 60-mm dish containing 2.5 ml of the enzyme solution, where it was dissected into small, cotton-like pieces using tweezers. These fragments were subjected to pipetting 20 to 30 times with a wide-bore pipette before being transferred to a 15-ml centrifuge tube containing 2.5 ml of stopping buffer, with further pipetting conducted approximately 20 times. A droplet was placed on the underside of a dish lid for microscopic examination to estimate the percentage of beating cardiomyocytes among the total cells. The solution was subsequently supplemented with stopping buffer to reach a final volume of 10 ml. Centrifugation at 20g for 5 min facilitated the sedimentation of cardiac myocytes, leaving the cardiac fibroblasts in the supernatant. The sediment was collected and resuspended in Krebs-bicarbonate solution and then kept on ice for further experimental procedures.

Adenoviral infection and siRNA transfection

For the in vitro experiments, recombinant adenoviruses expressing GFP or PRODH were used for exogenous expression of PRODH (Gene Pharma Co., Ltd., Shanghai, China). NRVMs were infected by adenoviruses after being cultured by serum-free DMEM for at least 12 hours [multiplicity of infection (MOI) = 50]. PE treatments were conducted after 24 hours of transfection. Knockdown of PRODH was conducted by transfection of siRNA using iMax transfection reagent (Thermo Fisher Scientific, Waltham, USA). Briefly, NRVMs were transfected by 50 μ M siRNA for 24 hours before PE treatment. The sequence of siRNA for PRODH was as follows: -GGACUAUGGUGUGGAGGAAdTdT and -UUCUCCACACCAUAGUCCdTdT.

Immunofluorescence staining

To determine the relative cell surface area of NRVMs, the F-actin cytoskeleton was stained using phalloidin-TRITC (red) (YEASEN, Shanghai, China). Briefly, The NRVMs were first fixed in 4% PFA for 10 min and then permeabilized with 0.1% Triton X-100 for 5 min at room temperature. The cells were subsequently stained with 100 nM TRITC-labeled phalloidin and mounted with anti-fade/4',6-diamidino-2-phenylindole (DAPI) mountant.

For WGA staining, frozen heart sections (5 μ m) were washed three times with PBS, then fixed with 4% PFA solution for 15 min at 37°C, and then stained with Alexa Fluor 594-WGA with a concentration of 10 μ g/ml (Thermo Fisher Scientific, Waltham, USA). After washing with PBS, the sections were mounted with anti-fade/DAPI mountant. The cross-sectional areas of cardiomyocytes were measured by Image J (v1.50).

To evaluate the ROS generated in the cells, DHE staining (YEASEN, Shanghai, China) was performed on the heart sections and NRVMs using a 10 μ M DHE solution at 37°C for 1 hour. The sections were then mounted with anti-fade/DAPI mountant after washing with PBS. The ratio of DHE-positive cells to the total amount of DAPI was calculated for the in vivo experiment, and the fluorescence intensity was measured for the in vitro experiment.

Electron microscopy

Freshly dissected cardiac tissues from the left ventricle of mice were dissected into pieces of approximately 1 mm² and immediately immersed in a 2.5% glutaraldehyde solution for fixation, followed by overnight incubation at 4°C. Subsequently, they were fixed with 1% osmium tetroxide, dehydrated in acetone, and embedded in epoxy resin. Next, the samples were sectioned into 70-nm slices using an ultramicrotome, followed by double staining with 3% uranyl acetate and lead citrate. Last, the prepared samples were observed using a JEM1230 transmission electron microscope (JEOL, Japan).

PRODH activity assay

The PRODH activity assay was performed using a commercial kit (Solarbio, Beijing, China). In brief, cardiac tissues were placed into an extraction solution and kept on ice, followed by centrifugation at 1500g for 15 min at 4°C. Subsequently, the additional prepared extraction solution was added, and the mixture was gently agitated for 30 min on ice. Next, the supernatant was collected by centrifugation at 15,000g for 20 min at 4°C and incubated at 37°C for 5 min. The absorbance of the samples or standard solutions was then measured at a wavelength of 600 nm using a spectrophotometer. Last, the detected PRODH activity was normalized according to the samples' mass.

GSH/GSSG ratio detection assay

To determine the relative GSH/GSSG of the NRVMs and AMCMs, a commercial detection assay kit was applied according to the manufacturer's instructions (Abcam, Cambridge, UK). Briefly, the supernatant of samples was collected after high-speed centrifugation for further analysis following the lysis of cells. The supernatant was mixed with an equal volume of assay reagent, and the mixture was incubated in the dark at room temperature for 1 hour before measuring the fluorescence intensity at 520 nm. By comparing the results with a standard curve, the contents of GSH and GSSG in NRVMs and AMCMs are determined, and the GSH/GSSG ratio is subsequently calculated.

Single-cell sequence analysis

The single-cell RNA-seq data for this study were obtained from GSE95140, including TAC-model mice at different stages (sham, 3 days, 1 week, and 4 weeks). Quality control and cell annotation were performed according to a prior study. R package Seurat (v4.1.3) was used for data integration, cell filtration, normalization, clustering, and *t*-distributed stochastic neighbor embedding (*t*-SNE) dimensional reduction. Monocle2 (v2.22.0) was used for cell pseudotime analysis. Cell progression genes were defined based on DEGs among Seurat clusters. Differential gene test function was used to explore gene dynamics during cell differentiation. Therefore, the trajectory was divided into five segments according to the trajectory nodes.

RNA-seq and bioinformatic analysis

The RNA-seq was performed by Novogene Company. The total RNAs of cardiac tissue or AMCMs were extracted by TRIzol reagent and quantified using the NanoDrop spectrophotometer. The quality of RNA was then evaluated with a standard protocol. RNA samples with sufficient quantity and high quality were subjected to library preparation. RNA-seq libraries were created using the Illumina HiSeq Stranded mRNA Library Prep Kit. The prepared libraries were sequenced on an Illumina NovaSeq 6000 according to the manufacturer's instructions. Raw sequencing data in FASTQ format were generated and subjected to quality control. Raw sequencing reads were preprocessed to remove low-quality bases, adaptors, and contaminants. The cleaned reads were aligned to *Mus musculus* using STAR with default parameters. The aligned reads were sorted and indexed for downstream analysis. Gene expression levels were quantified based on the read counts mapped to each gene. Differential gene expression analysis was performed using DESeq2. Genes with adjusted *P* values below a pre-defined threshold (FDR < 0.05) were considered as DEGs. Functional annotation and pathway enrichment analysis of DEGs were conducted using the KEGG database. Pathways substantially enriched with DEGs were identified using DAVID. Visualization of enriched pathways and related genes was performed using R packages.

Nontargeted metabolite profiling and bioinformatics

In this study, nontargeted metabolite profiling was conducted by Panomix Biotech Company (Suzhou, China). The collection of samples, specifically NRVMs post-treatment, adhered to the manufacturer's standard protocol. Metabolite extraction was performed using 80% methanol to encompass a wide spectrum of metabolites, with an optimized extraction process to maximize recovery. Following extraction, samples were subjected to vortexing and subsequent centrifugation to segregate the organic and aqueous phases. The extracted metabolites were then lyophilized for subsequent liquid chromatography–mass spectrometry (LC-MS) analysis. LC-MS analysis was executed using high-performance liquid chromatography coupled with a quadrupole orthogonal acceleration–time-of-flight mass spectrometer. Instrument calibration was carried out according to the manufacturer's recommendations. Chromatographic separation was achieved using a mobile phase, with optimization of chromatographic parameters including flow rate and gradient to enhance metabolite separation. Mass spectrometry analysis was performed in both positive and negative ionization modes, acquiring full-scan spectra over a predefined mass range. The raw LC-MS data generated during the analysis were stored in a standardized format established by Panomix Biotech Company. These raw data files were subsequently subjected to preprocessing steps, including peak detection, alignment, and retention time correction. Detected features were annotated by referencing available spectral databases to facilitate metabolite identification. Differential metabolite analysis was conducted using statistical tools, applying appropriate tests to identify notable differences between experimental groups. Furthermore, pathway enrichment analysis of the DEMs was carried out to discern metabolic pathways associated with these alterations. It is noteworthy that all data analyses described herein were conducted within the BioDeep cloud analysis platform.

Seahorse assay

The OCR assessment of NRVMs was executed using an Agilent Seahorse XFe 96 Extracellular Flux Analyzer, adhering strictly to the manufacturer's guidelines. The experiment was initiated by seeding

the NRVMs on XFe 96 cell culture microplates with DMEM. This was followed by transfection of the cells with Ad-PRODH and subsequent induction with PE. On the day of the experiment, the hydration plate was meticulously rinsed twice with a calibration solution, followed by incubation in a 37°C culture incubator for 45 min. Subsequently, the NRVMs were washed twice with XFe 96–configured medium and incubated in a 37°C culture incubator for 1 hour. The subsequent step involved the addition of oligomycin (1.5 μM), carbonyl cyanide *p*-(trifluoromethoxy) phenylhydrazone (2.0 μM), and a combination of rotenone and antimycin A (0.5 μM) into the probe plate, which was subsequently introduced into the analyzer for calibration. Upon successful calibration, the incubated cells were transferred onto the probe plate to facilitate the final determination of the OCR.

ATP content assay

The ATP content measurement was conducted using a commercial kit (Beyotime, Haimen, China). NRVMs were seeded in six-well plates and subsequently received different treatments. At the end of the treatment, 200 μl of lysis buffer was added to each well of the six-well plate. Subsequently, the lysates were centrifuged at 12,000g for 5 min at 4°C, and the supernatants were collected for subsequent assays. Next, 100 μl of ATP working solution was added into detection tubes incubated at room temperature for 3 to 5 min. Following this, 20 μl of the test supernatant or standard solution was added and mixed. Last, the relative light units of each sample were measured using a luminometer. Simultaneously, the supernatant from each sample was used for protein quantification to normalize the ATP content to micrograms of protein.

L-Proline-¹³C5, ¹⁵N stable isotope tracing analysis

The NRVMs were initially seeded on six-well plates. After 12 hours of serum-free culture, the cells were transfected with Ad-GFP or Ad-PRODH for 24 hours. Subsequently, a specialized culture medium for isotope experiments was prepared, consisting of serum-free, glucose-free, and glutamine-free DMEM; 25 mM D-glucose; 4 mM glutamine; and 2 mM L-proline. PE (100 μM) was added to this medium to stimulate cardiomyocytes for 48 hours. Upon completion of the cell treatment, cardiomyocytes were washed twice with a pre-cooled 0.9% sodium chloride solution. The cells were then extracted with –80°C pre-cooled 80% methanol. The collected cells were subjected to enzyme inactivation at –80°C overnight. Afterward, the supernatant was then dried by a vacuum concentrator and stored at –80°C for further LC-MS analysis. The protein concentration was determined by dissolving the sediment with 200 mM NaOH. The isotope tracing analysis was performed by Lipid ALL. High-resolution mass spectrometry coupled with liquid chromatography was used to analyze ¹³C metabolites. LC-MS data acquisition, raw data analysis, and normalization were performed using LC-MS peak intensities (integral peak area) to calculate the relative abundance ratio of each metabolite. For individual metabolites, the ¹³C isotopic distribution was determined using the peak intensities of each ¹³C isotope.

RNA isolation, cDNA synthesis, and quantitative RT-PCR

Total RNA from NRVMs or mouse left ventricle tissue was extracted using the RNA quick purification kit (Esunbio Co., Ltd., Shanghai, China). The RNA was then reverse-transcribed for cDNA synthesis by the PrimeScript™ RT Master Mix (Takara, Tokyo, Japan). Quantitative RT-PCR was performed to determine the relative mRNA

expression of target genes using the Hieff UNICON qPCR SYBR Green Master Mix (YEASON, Shanghai, China) on the Vii7 system (Applied Biosystems, CA, USA). All primer sequences of target genes are listed in table S5.

Western blotting assay

The protein isolation from the animal tissue was performed using a tissue grinder. Briefly, heart tissues were lysed in the buffer with radioimmunoprecipitation assay (RIPA) buffer and Phenylmethylsulfonyl fluoride (PMSF) (100:1). The whole lysates were then collected by the tissue grinder. For the extraction of protein from cultured cells, the cells were first washed with cold PBS twice and lysed with 100 μl of RIPA and PMSF (100:1) for each well. After the centrifugation at 12,000 rpm for 15 min, the supernatants were collected for the bicinchoninic acid assay (Beyotime, Haimen, China). Then, the protein samples were boiled for 5 min at 100°C. The same amounts of proteins of each sample were loaded onto the SDS–polyacrylamide gel electrophoresis gels (Fude Biological Technology, Hangzhou, China) for electrophoresis, followed by transferring to the 0.22-μm polyvinylidene fluoride membrane (Bio-Rad, CA, USA) with a constant current of 250 mA for 2 hours. The membrane was then blocked by the 5% nonfat milk for 1 hour at room temperature, followed by incubating with corresponding primary antibodies overnight at 4°C. The primary antibodies used in this study are listed as follows: ANP (27426-1-AP, Proteintech), PRODH (22980-1-AP, Proteintech), β-MHC (22280-1-AP, Proteintech), p-S6K (T389) (9234, CST), S6K (34475, CST), p-4E-BP1 (S65) (9451, CST), 4E-BP1 (9452, CST), GCLC (12601-1-AP, Proteintech), GSR (18257-1-AP, Proteintech), and GAPDH (HRP-60004, Proteintech). After incubating with secondary anti-rabbit (70-GAM0072, MultiSciences) or anti-mouse (70-GAM007, MultiSciences) antibodies, the bands were detected by electrochemiluminescence reagents (Beyotime, Haimen, China) by the Amersham Imager 600 system (GE Healthcare, Buckinghamshire, England).

Statistical analysis

All data in this study are expressed as means ± SEM. Statistical analysis was performed with Prism 8.0 (GraphPad Software, Inc.). Student's unpaired *t* test was performed for the comparison between the two groups. One-way ANOVA followed by Bonferroni post-hoc test was performed by comparison among three or more groups when involving one factor. Two-way ANOVA with Bonferroni post-hoc test was used for the four-group comparison when involving two factors. *P* < 0.05 was considered as a statistical difference in this study. Statistical analyses were performed using GraphPad Prism (8.0).

Supplementary Materials

This PDF file includes:

Figs. S1 to S8
Tables S1 to S5

REFERENCES AND NOTES

1. K. T. Mills, A. Stefanescu, J. He, The global epidemiology of hypertension. *Nat. Rev. Nephrol.* **16**, 223–237 (2020).
2. I. Shimizu, T. Minamino, Physiological and pathological cardiac hypertrophy. *J. Mol. Cell. Cardiol.* **97**, 245–262 (2016).
3. T. Tuomainen, P. Tavi, The role of cardiac energy metabolism in cardiac hypertrophy and failure. *Exp. Cell Res.* **360**, 12–18 (2017).
4. S. Saheera, P. Krishnamurthy, Cardiovascular changes associated with hypertensive heart disease and aging. *Cell Transplant.* **29**, 963689720920830 (2020).

5. E. Packard, A. de Feria, S. Peshin, N. Reza, A. T. Owens, Contemporary therapies and future directions in the management of hypertrophic cardiomyopathy. *Cardiol. Ther.* **11**, 491–503 (2022).
6. J. Ritterhoff, R. Tian, Metabolic mechanisms in physiological and pathological cardiac hypertrophy: New paradigms and challenges. *Nat. Rev. Cardiol.* **20**, 812–829 (2023).
7. C. M. Sag, C. X. C. Santos, A. M. Shah, Redox regulation of cardiac hypertrophy. *J. Mol. Cell. Cardiol.* **73**, 103–111 (2014).
8. G. D. Lopaschuk, Q. G. Karwi, R. Tian, A. R. Wende, E. D. Abel, Cardiac energy metabolism in heart failure. *Circ. Res.* **128**, 1487–1513 (2021).
9. Q. Li, C. Li, A. Elnwasany, G. Sharma, Y. An, G. Zhang, W. M. Elhelaly, J. Lin, Y. Gong, G. Chen, M. Wang, S. Zhao, C. Dai, C. D. Smart, J. Liu, X. Luo, Y. Deng, L. Tan, S. J. Lv, S. M. Davidson, J. W. Locasale, P. L. Lorenzi, C. R. Malloy, T. G. Gillette, M. G. Vander Heiden, P. E. Scherer, L. I. Szewda, G. Fu, Z. V. Wang, PKM1 exerts critical roles in cardiac remodeling under pressure overload in the heart. *Circulation* **144**, 712–727 (2021).
10. A. R. Wende, J. Kim, W. L. Holland, B. E. Wayment, B. T. O'Neill, J. Tuinei, M. K. Brahma, M. E. Pepin, M. A. McCrory, I. Luptak, G. V. Halade, S. E. Litwin, E. D. Abel, Glucose transporter 4-deficient hearts develop maladaptive hypertrophy in response to physiological or pathological stresses. *Am. J. Physiol. Heart Circ. Physiol.* **313**, H1098–h1108 (2017).
11. S. C. Kolwicz Jr., R. Tian, Glucose metabolism and cardiac hypertrophy. *Cardiovasc. Res.* **90**, 194–201 (2011).
12. S. C. Kolwicz Jr., D. P. Olson, L. C. Marney, L. Garcia-Menendez, R. E. Synovec, R. Tian, Cardiac-specific deletion of acetyl CoA carboxylase 2 prevents metabolic remodeling during pressure-overload hypertrophy. *Circ. Res.* **111**, 728–738 (2012).
13. L. Burke, I. Guterman, R. Palacios Gallego, R. G. Britton, D. Burschowsky, C. Tufarelli, A. Rufini, The Janus-like role of proline metabolism in cancer. *Cell Death Discov.* **6**, 104 (2020).
14. J. M. Phang, Proline metabolism in cell regulation and cancer biology: Recent advances and hypotheses. *Antioxid. Redox Signal.* **30**, 635–649 (2019).
15. J. Pandhare, S. P. Donald, S. K. Cooper, J. M. Phang, Regulation and function of proline oxidase under nutrient stress. *J. Cell. Biochem.* **107**, 759–768 (2009).
16. M. Yam, A. L. Engel, Y. Wang, S. Zhu, A. Hauer, R. Zhang, D. Lohner, J. Huang, M. Dinterman, C. Zhao, J. R. Chao, J. Du, Proline mediates metabolic communication between retinal pigment epithelial cells and the retina. *J. Biol. Chem.* **294**, 10278–10289 (2019).
17. W. Liu, J. M. Phang, Proline dehydrogenase (oxidase) in cancer. *Biofactors* **38**, 398–406 (2012).
18. W. Liu, A. Le, C. Hancock, A. N. Lane, C. V. Dang, T. W. Fan, J. M. Phang, Reprogramming of proline and glutamine metabolism contributes to the proliferative and metabolic responses regulated by oncogenic transcription factor c-MYC. *Proc. Natl. Acad. Sci. U.S.A.* **109**, 8983–8988 (2012).
19. P. J. Kennel, X. Liao, A. Saha, R. Ji, X. Zhang, E. Castellero, D. Brunjes, H. Takayama, Y. Naka, T. Thomas, I. George, D. Mancini, P. C. Schulze, Impairment of myocardial glutamine homeostasis induced by suppression of the amino acid carrier SLC1A5 in failing myocardium. *Circ. Heart Fail.* **12**, e006336 (2019).
20. M. J. Ranek, K. M. Kokkonen-Simon, A. Chen, B. L. Dunkerly-Eyring, M. P. Vera, C. U. Oeing, C. H. Patel, T. Nakamura, G. Zhu, D. Bedja, M. Sasaki, R. J. Holewinski, J. E. Van Eyk, J. D. Powell, D. I. Lee, D. A. Kass, PKG1-modified TSC2 regulates mTORC1 activity to counter adverse cardiac stress. *Nature* **566**, 264–269 (2019).
21. D. H. Tran, H. I. May, Q. Li, X. Luo, J. Huang, G. Zhang, E. Niewold, X. Wang, T. G. Gillette, Y. Deng, Z. V. Wang, Chronic activation of hexosamine biosynthesis in the heart triggers pathological cardiac remodeling. *Nat. Commun.* **11**, 1771 (2020).
22. Z. K. Haque, D. Z. Wang, How cardiomyocytes sense pathophysiological stresses for cardiac remodeling. *Cell. Mol. Life Sci.* **74**, 983–1000 (2017).
23. F. L. Sheeran, S. Pepe, Energy deficiency in the failing heart: Linking increased reactive oxygen species and disruption of oxidative phosphorylation rate. *Biochim. Biophys. Acta* **1757**, 543–552 (2006).
24. A. A. Gibb, B. G. Hill, Metabolic coordination of physiological and pathological cardiac remodeling. *Circ. Res.* **123**, 107–128 (2018).
25. H. Sun, K. C. Olson, C. Gao, D. A. Prosdocimo, M. Zhou, Z. Wang, D. Jeyaraj, J. Y. Youn, S. Ren, Y. Liu, C. D. Rau, S. Shah, O. Ilkayeva, W. J. Gui, N. S. Williams, R. M. Wynn, C. B. Newgard, H. Cai, X. Xiao, D. T. Chuang, P. C. Schulze, C. Lynch, M. K. Jain, Y. Wang, Catabolic defect of branched-chain amino acids promotes heart failure. *Circulation* **133**, 2038–2049 (2016).
26. J. Ritterhoff, S. Young, O. Villet, D. Shao, F. C. Neto, L. F. Bettcher, Y. A. Hsu, S. C. Kolwicz Jr., D. Raftery, R. Tian, Metabolic remodeling promotes cardiac hypertrophy by directing glucose to aspartate biosynthesis. *Circ. Res.* **126**, 182–196 (2020).
27. L. Xu, M. Brink, mTOR, cardiomyocytes and inflammation in cardiac hypertrophy. *Biochim. Biophys. Acta* **1863**, 1894–1903 (2016).
28. J. B. N. Moreira, M. Wohlwend, S. Fenk, I. Åmellem, A. Flatberg, J. Kraljevic, J. Marinovic, M. Ljubkovic, G. Bjørkøy, U. Wisløff, Exercise reveals proline dehydrogenase as a potential target in heart failure. *Prog. Cardiovasc. Dis.* **62**, 193–202 (2019).
29. K. Sugamura, J. F. Keaney Jr., Reactive oxygen species in cardiovascular disease. *Free Radic. Biol. Med.* **51**, 978–992 (2011).
30. H. Tsutsui, S. Kinugawa, S. Matsushima, Oxidative stress and heart failure. *Am. J. Physiol. Heart Circ. Physiol.* **301**, H2181–H2190 (2011).
31. L. A. Vettore, R. L. Westbrook, D. A. Tennant, Proline metabolism and redox; maintaining a balance in health and disease. *Amino Acids* **53**, 1779–1788 (2021).
32. S. K. Natarajan, W. Zhu, X. Liang, L. Zhang, A. J. Demers, M. C. Zimmerman, M. A. Simpson, D. F. Becker, Proline dehydrogenase is essential for proline protection against hydrogen peroxide-induced cell death. *Free Radic. Biol. Med.* **53**, 1181–1191 (2012).
33. J. Wang, Z. Xue, J. Lin, Y. Wang, H. Ying, Q. Lv, C. Hua, M. Wang, S. Chen, B. Zhou, Proline improves cardiac remodeling following myocardial infarction and attenuates cardiomyocyte apoptosis via redox regulation. *Biochem. Pharmacol.* **178**, 114065 (2020).
34. J. Wang, Z. Xue, C. Hua, J. Lin, Z. Shen, Y. Song, H. Ying, Q. Lv, M. Wang, B. Zhou, Metabolomic analysis of the ameliorative effect of enhanced proline metabolism on hypoxia-induced injury in cardiomyocytes. *Oxid. Med. Cell. Longev.* **2020**, 8866946 (2020).
35. N. Quan, X. Li, J. Zhang, Y. Han, W. Sun, D. Ren, Q. Tong, J. Li, Substrate metabolism regulated by Sestrin2-mTORC1 alleviates pressure overload-induced cardiac hypertrophy in aged heart. *Redox Biol.* **36**, 101637 (2020).
36. R. F. Chi, L. Li, A. L. Wang, H. Yang, J. Xi, Z. F. Zhu, K. Wang, B. Li, L. G. Yang, F. Z. Qin, C. Zhang, Enhanced oxidative stress mediates pathological autophagy and necroptosis in cardiac myocytes in pressure overload induced heart failure in rats. *Clin. Exp. Pharmacol. Physiol.* **49**, 60–69 (2022).
37. J. Lin, Q. Li, T. Jin, J. Wang, Y. Gong, Q. Lv, M. Wang, J. Chen, M. Shang, Y. Zhao, G. Fu, Cardiomyocyte IL-1R2 protects heart from ischemia/reperfusion injury by attenuating IL-17RA-mediated cardiomyocyte apoptosis. *Cell Death Dis.* **13**, 90 (2022).
38. T. D. O'Connell, M. C. Rodrigo, P. C. Simpson, Isolation and culture of adult mouse cardiac myocytes. *Methods Mol. Biol.* **357**, 271–296 (2007).

Acknowledgments

Funding: This work was supported by the National Natural Science Foundation of China [82200271 (M.S.), 82311530688 (M.S.), 82270262 (W.Z.), and 82070408 (W.Z.)] and the Natural Science Foundation of Zhejiang Province, People's Republic of China [LY23H020005 (W.Z.) and LQ22H020010 (M.S.)]. **Author contributions:** Conceptualization: W.Z., M.S., and G.F. Methodology: M.S., Q.Z., and Y.W. Investigation: Q.L., D.L., L.Z., and P.Y. Visualization: D.L. and Y.T. Supervision: G.F., W.Z., M.S., and M.W. Writing—original draft: Q.L. and D.L. Writing—review and editing: M.S. and W.Z. **Competing interests:** The authors declare that they have no competing interests. **Data and materials availability:** All data needed to evaluate the conclusions in the paper are present in the paper and/or the Supplementary Materials.

Submitted 7 November 2023

Accepted 4 April 2024

Published 8 May 2024

10.1126/sciadv.adl3549